From the Klinik für Innere Medizin III
mit den Schwerpunkten Kardiologie, Angiologie und internistische Intensivmedizin
(interim direktor: Prof. Dr. med. Derk Frank)
at the University Medical Center Schleswig-Holstein, Campus Kiel
at Kiel University

The Krüppel-Like Factor 4 as a novel gene therapy target for Hypoxic Pulmonary Hypertension

Dissertation
to acquire the doctoral degree (Dr. med.)
at the Faculty of Medicine
at Kiel University

presented by

Yi Lyu
from **Shanxi, China**
Kiel, **2021**

1st Reviewer: Prof. Dr. med. Oliver Müller

2nd Reviewer: Priv.-Doz. Dr. Thomas Pühler

Date of the oral examination: 21.11.2022

Approved for printing, Kiel

Signed: Prof. Dr. Derk Frank

(Chairperson of the Examination Committee)

Declaration:

I hereby declare that this thesis is my own work in content and form, except for my supervisor's advice. I further declare that the study was written following the good scientific practice of the German Research Foundation. This study has not yet been submitted, published, or submitted for publication, neither in part nor in full, to any other institution in the context of an examination procedure. Furthermore, I declare that I have not yet undertaken any previous attempts at a doctorate.

_____ _____

City, Date Yi Lyu

Contents

Abbreviations

°C	Grad Celsius
AAVs	Adeno-associated virus
AF	Alexa Fluor®- fluorescent dye
AngII	Angiotensin II
ANOVA	analysis of variance
APS	Ammonium persulfate
BBB	blood-brain barrier
BSA	Bovine Serum Albumin
Ca^{2+}	Calcium
CD31	Platelet endothelial cell adhesion molecule
cDNA	Complementary DNA
CLD	Chromic-Lung Disease
CMV	Cytomegalovirus
CNS	the central nervous system
CO2	carbon dioxide
Co-IP	Co-Immunoprecipitation
COPD	Chronic obstructive pulmonary disease
COX2	Cyclooxygenase-2
CRF	corticotropin-releasing factors
DAPI	4′,6-Diamidin-2-phenylindole
ddH_2O	Double distilled water
DEPC	Diethyl pyrocarbonate
DMEM	Dulbecco's Modified Eagle Medium
DMSO	Dimethyl sulfoxide
DNA	Deoxyribonucleic acid
dNTP	Deoxyribonucleoside triphosphate
DTT	Dithiothreitol
E. coli	Escherichia coli
EC	Endothelial cell
ECL	Enhanced Chemiluminescence
EGFP	Enhanced green fluorescent protein
EndMT	Endothelial-mesenchymal transition
eNOS	endothelial oxide synthesis

ESC	European Society of Cardiology
Fig	Figure
FITC	Fluorescein Isothiocyanate
Fw	forward
g	Gramm
GAPDH	Glyceraldehyde-3-phosphate-Dehydrogenase
h	Hour
H_2O_2	Hydrogen peroxide
HIF1α	Hypoxia-inducible factor 1-alpha
HPH	Hypoxic Pulmonary Hypertension
HRP	Horseradish Peroxidase
hs	homo sapiens
HSPs	Heat shock proteins
HUVECs	Human umbilical vein endothelial cells
ICAM-1	intercellular adhesion molecule-1
IF	Immunofluorescence
ifu	Infectious units
IL-1β	interleukin-1 beta
IL-6	Interleukin-6
kb	Kilobase pair
kDa	Kilo Dalton
KEGG	Kyoto Encyclopedia of Genes and Genomes
KLF	Krüpple-Like factor
l	Liter
M	Molar
MAPK	Mitogen-Activated Protein Kinase
MCP-1	monocyte chemoattractant protein-1
MgCl2	Magnesium chloride
min	minute
miRNA	micro-RNA
ml	Milliliter
mm	Mus musculus
MMP	Matrix-Metalloproteinase
MOI	multiplicity of infection

mRNA	messenger RNA
MW	Molecular weight
NaCl	Sodium chloride
NFκB	nuclear factor kappa-light-chain-enhancer of activated B cells
nm	Nanometer
NOS	nitric oxide synthesis
OD	Optical density
OE	overexpression
p21	cyclin-dependent kinase inhibitor 1
PAH	Pulmonary arterial hypertension
PBS	Phosphate Buffered Saline
PCR	Polymerase Chain Reaction
PE	Phenylephrine
PFA	Paraformaldehyde
PGI2	Prostacyclin
PH	Pulmonary Hypertension
pH	Negative logarithm of the hydronium ion concentration
PINK1	PTEN-induced kinase 1
PVDF	Polyvinyl difluoride
qPCR	Quantitative Real-Time PCR
RNA	Ribonucleic acid
ROS	reactive oxygen species
rpm	Revolutions per minute
RT	Room temperature
Rv	reverse
S	Seconds
SD	Standard deviation
SDB	Obstructive sleep-disordered breathing
SDS	Sodiumdodecylsulfate
SMA	smooth muscle actin
SOD2	Superoxide-Dismutase 2
SV40	Simian Virus 40

TBST	Tris-Buffered Saline Tween 20
TEMED	Tetramethylethylendiamine
TF	Transcription factor
TGF-β	transforming growth factor β
TNFα	Tumornekrosefaktor-α
Tris	tris(hydroxymethyl)aminomethane
Triton X-100	Polyethylene glycol *p*-(1,1,3,3-tetramethylbutyl)-phenyl ether
U	Units
UV	Ultraviolet
v/v	Volume/Volume
VCAM-1	vascular cell adhesion molecule-1
VSMC	vascular smooth muscle cell
vWF	von Willebrand factor
w/v	Weight/Volume
WB	Western Blot
WHO	World Health Organization
X g	Centrifugal force
ZFN	zinc-finger nuclease
ZO-1	tight junction protein 1

List of Tables

List of Figures

1. Introduction

1.1 Pulmonary Hypertension

1.1.1 Overview

Pulmonary hypertension (PH) is a cardiovascular and respiratory disease that can result in multiple complications(1). PH is associated with increased morbidity and mortality life-threatening illness. PH is characterized by increased pulmonary vascular resistance and venous pressure as pathophysiological features(2). PH is assessed by right heart catheterization (RHC) and defined as an increase in mean pulmonary artery pressure (mPAP) to 20 mmHg or more at rest, or 30 mmHg during physical activity, compared with the expected average level of approximately 14.0±3.3 mmHg at rest(3). The pulmonary arteries are responsible for transporting blood from the right ventricle to the lungs. But if the normal physiological state is disrupted, the pulmonary arteries' walls are thickened and stiffened, and the vessel lumen is narrowed or occluded(4). As the disease progresses, various organs will gradually fail, and clinical manifestations will appear. The most common symptoms are shortness of breath/dyspnea, fatigue, dizziness or syncope, pressure and pain in the chest, swelling in the ankles, legs, or abdomen, bluish color in the lips, and skin/ cyanosis, arrhythmias(5). PH is a progressive disease, and its symptoms get worse with time. The disease's presentation varies depending on the characteristics of the patient and the subtype of the disease(5).

1.1.2 Classification

According to the clinical manifestations and pathology, PH is categorized into five groups(5). Group 1 is Pulmonary arterial hypertension (PAH), and Group 2 is Pulmonary hypertension due to left heart disease (PH-LHD). Group 3 is Pulmonary hypertension due to chronic lung disease (CLD-PH) and/or hypoxia (HPH), and Group 4 is Chronic thromboembolic pulmonary hypertension (CTEPH). Group 5 is Pulmonary hypertension with unclear and/or multifactorial mechanisms. Pulmonary hypertension due to chronic lung disease (CLD-PH) and/or hypoxia (HPH) is the main focus of this study.

1.1.3 Pathophysiology of pulmonary hypertension

1.1.3.1 Hypoxia effects on pulmonary arteries

Oxygen homeostasis is essential for the proper physiological function of the organism(6). For this reason, the body has developed regulatory mechanisms that allow for adequate oxygen supply to satisfy the metabolic needs of the cell. When these mechanisms fail, and the intracellular oxygen concentration decreases, a state of hypoxic stress occurs. Hypoxia is physiological stress associated with many physio-pathological processes such as cancer, high altitude adaptation, or hypoxic pulmonary hypertension(3).

In response to hypoxia, the most essential developmental and physiological responses are hypoxic vasoconstriction and pulmonary vascular remodeling(6). Endothelial vascular remodeling occurs in the pulmonary vasculature during chronic hypoxia. The endothelial cells (ECs) and the smooth muscle cells (SMCs) are intricately related in various physiological processes and work in close coordination to maintain the stability of vascular function. The ECs layer works like a permeable barrier separating the circulating blood cells from the vascular tissue. Its unique position responds to cytokines and functions as a signal collector and convertor, effectively controlling the vascular function(7). Hypoxia leads to endothelial dysfunction. It presents increasing pulmonary vascular permeability, disrupting the balance between vasoconstriction and vasodilation, releasing inflammatory mediators and oxidative stress by activating pro-inflammatory phenotypes.

Endothelial-to-mesenchymal transition (EndMT) is a typical and potentially disease-causal biological program by which endothelial cells transform into mesenchymal cells, such as endothelial cells, transform into myofibroblasts or smooth muscle cells(8). All vascular layers (adventitia, media, neointima) are thickening and present dysfunctional vasodilatation and vasocontraction. EndMT plays a critical role in this program(9). The release of inflammatory factors manifests it, activating reactive oxygen species (ROS) and TGF-β signaling, increased secretion of cytokines, and infiltration of leukocytes. In the presence of hypoxia, pulmonary vascular cells secrete pro-inflammatory cytokines (IL-1, IL-6, TNFα). EndMT is typically characterized by decreased endothelial gene/protein (CD31, Tie2, vWF, VE-Cadherin, ZO-1) expression and an increase in mesenchymal gene/protein (vimentin, α-SMA, SM22α) expression. Oxidative stress is another factor that supports EndMT. Hypoxia regulates the expression of hydrogen peroxide (H2O2) and induces oxidative stress to accelerate

EndMT(10). Besides, hypoxia causes inhibition of nitric oxide synthesis (NOS), which negatively regulates oxidative stress, also contributing to EndMT.

1.1.3.2 Hypoxia effects on mitochondria

Mitochondria are the main sites of oxidative phosphorylation and synthesis of the Adenosine triphosphate (ATP)(11). The mitochondria provide chemical energy for cavities and participate in cell differentiation, messaging, cell growth, or apoptosis. Pathophysiological changes in pulmonary hypertension are associated with multiple mechanisms of mitochondrial dysfunction(12). Most of these mechanisms are linked to each other. Persistent hypoxia can lead to mitochondrial electron transport chain (ETC) dysfunction that causes less ATP production and increases mitochondrial ROS. Meanwhile, mitochondrial DNA was damaged, cooperated with ROS, initiated apoptosis, impaired biogenesis, or changed mitochondrial structure or morphology. These disturbances in mitochondrial function and/or biogenesis play a crucial role in developing pulmonary hypertension.

1.1.3.3 Hypoxia-induced inflammation

Oxygen deprivation induces an increase in pro-inflammatory cytokines and vascular leakage, as evidenced by increased serum levels of interleukin-1 beta (IL-1β), interleukin-6 (IL-6), C-reactive protein, Tumor Necrosis Factor-α (TNF-α), as well as other inflammatory markers(13). Hypoxia can activate the nuclear factor-kappa B (*NF-κB*) and thus upregulates the expression of various interleukins (IL), including IL-1, IL-6, transforming growth factor-beta (TGF-β), and tumor necrosis factor (TNF-α)(14). IL-6 is an oxygen-regulated protein synthesized and released on hypoxia-exposed endothelial cells while suppressing IL-1 and TNF-α expressions. TGF-β is a multifunctional secreted protein that activates cell growth, proliferation, differentiation, and apoptosis. It leads to the up-regulation of adhesion molecules on the surface of HUVEC. Intracellular adhesion molecule 1 (ICAM-1) as a transmembrane protein presents in endothelial cell membranes(15). ICAM-1 can be evoked by interleukin-1 (IL-1) and tumor necrosis factor (TNF) and presents a rapid and sustained reaction upon the little oxygen stimulation. Vascular cell adhesion protein 1 (VCAM-1) mediates the adhesion at the leukocyte-endothelial cell interphase. In response to cytokines, VCAM-1 expression is upregulated in endothelial cells. Of note, the available tandem *NF-κB* sites that induce various proinflammation genes are located in the promoter region of the *VCAM-1* gene(14). In other words, *VCAM-1* expression plays a critical role in inflammation. Monocyte chemoattractant

protein 1(MCP1), also known as chemokine ligand 2 (CCL2), mediates monocytes' migration and attracts monocytes into the foci of active inflammation(16). Increased MCP1 level indicates the activation of inflammation(16). Cyclooxygenase-2 (COX2) is a well-known enzyme that acts as a pro-inflammatory agent by activating prostaglandins. In short, inhibition of COX2 reduces prostaglandins production, and thus, has an anti-inflammatory effect(17).

1.1.3.4 Reactive oxygen species (ROS) in Hypoxia-induced pulmonary hypertension

ROS production is thought to be an essential signal for pulmonary vasoconstriction. Under normoxia, ROS in mitochondria is cleared by the antioxidant system. However, under hypoxic conditions, ROS production is usually increased(18). Acute short-term hypoxia activates antioxidant factors, which effectively inhibit the increase of ROS. Chronic hypoxia, on the other hand, allows ROS production, while the antioxidant mechanisms are inhibited(19). Thus, in chronic hypoxic pulmonary hypertension, ROS are abundantly expressed. Cellular respiration plays an essential role as a source of ROS in HPH(20). Hypoxic stimulation causes mitochondria to produce ROS that acts as activators of proline-4-hydroxylase, which induces the activation of hypoxia-inducible factor 1 (HIF-1), which triggers vascular remodeling and stenosis of the pulmonary artery(21).

1.1.3.5 HIF1-α signaling in Hypoxia pulmonary hypertension

Hypoxia-inducible factor (HIF) is a cellular enzyme responsible for initiating transcription of many hypoxia-induced genes(21). HIF contains two subunits, an oxygen-sensitive alpha subunit, and a constitutive beta subunit. HIF1-alpha is the most common alpha subunit, whose breakdown is associated with prolyl hydroxylase. The prolyl hydroxylase domain activity depends on oxygen, and the lack of oxygen leads to a decrease in its action and inhibition of HIF1-α. The HIF1-α effects on DNA are also dependent on oxygen concentration, and a deficiency of oxygen alters its activity and stability. Activation of the HIF-1 transcription factor is the most recognized pathway adopted by hypoxic cells. In addition, HIF-1 induces the expression of several pro-angiogenic factors such as the vascular endothelial growth factor (VEGF), NOS, transforming growth factor-beta (TGF-β). Altogether, HIF-1 activation is one of the key masters orchestrating their adaptation mechanisms to the hypoxia environment.

1.1.3.6 Nitric oxide signaling in Hypoxia pulmonary hypertension

Nitric oxide is produced by constitutive endothelium and inducible nitric oxide synthase (NOS)(22). Nitric oxide reduces Ca^{2+} and myofilament calcium sensitivity, relaxing the vascular smooth muscle and maintaining the pulmonary vessels in an actively dilated state. Nitric oxide synthesis is reduced under hypoxic conditions. The nitric oxide (NO) is synthesized by endothelial NOS (eNOS) and secreted by vascular endothelium for maintaining vascular homeostasis. Reduced NO generation contributes to endothelial dysfunction—hypoxia-induced endothelial dysfunction results in reduced NO production through reduced eNOS release. As a result, NO bioavailability and signaling are diminished in HPH.

1.1.4 Current therapy for hypoxia pulmonary hypertension and deficiencies

As the primary treatment option for chronic hypoxic pulmonary hypertension, there is no doubt that oxygen therapy is the best treatment for the underlying lung disease. Patients with hypoxemic lung disease with PH should receive long-term O_2 therapy(5). Although there are currently several options for PAH's pharmacological treatment, it is essential to note that patients with PH due to lung disease are not recommended to use the drugs approved for PAH. Therefore, there are currently no active therapeutic agents for chronic lung disease/hypoxic pulmonary hypertension besides long-term oxygen therapy.

1.2 Krüppel-Like Factor (KLF) 4

1.2.1 Identification of KLF4

The Krüppel-Like Factors (KLFs) are transcription factors named by its founder, containing the three C2H2-type zinc fingers with DNA-binding domains shared by KLF-like factors. Krüppel is a German word called for this protein as its homozygous resulted in Drosophila embryos' death by altering anterior abdominal and thoracic segments(23). The first mammalian Krüppel-Like Factor was KLF1, and also called erythroid Krüppel-Like Factor (EKLF), because it was identified in red blood cells. KLF4, gut-enriched KLF (GKLF), was initially identified in gut and skin epithelium(24). The main feature of *KLF4* is that it contains three domains: DNA binding domain, transcription regulation domain, and nuclear localization sequence. The highly conserved DNA binding domain is located at C-terminal and forms three C2H2 zinc fingers to regulate DNA binding specificity(25). In contrast, the

highly denatured transcriptional regulation domain is located at the N-terminus and mainly plays transcriptional activation and repression.

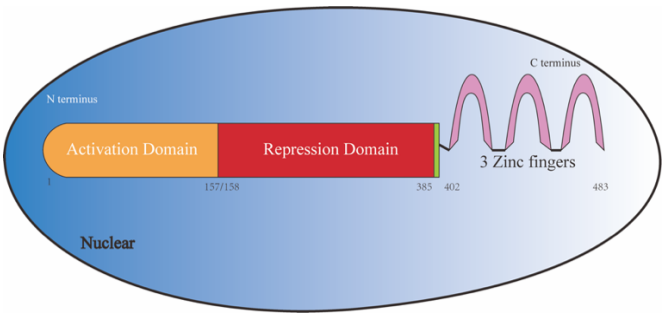

Figure 1. Structure of the *KLF4* gene

*KLF*4 is a transcriptional factor located in nuclear. The main feature of *KLF4* is the three C2H2-type zinc fingers with DNA-binding domains.

1.2.2 Biological aspects

Previous studies implicated that the deletion of *KLF4* could cause unwanted outcomes for the host. Lack of the *KLF4* gene causes the loss of skin barrier function that led to neonatal death(26). *KLF4* is highly expressed in various epidermis layers, such as gastrointestinal epithelium and corneal epithelial(27). *KLF4* in endothelial cells was first cloned from an endothelial cell library by Yet *et.al*(28). Subsequent efforts have elucidated that KLF4 is a regulator of endothelial activation induced by pro-inflammatory stimuli and shear stress. These studies also showed that overexpression of KLF4 induces several anti-inflammatory and anti-thrombotic factors that significantly decrease inflammation, reduce cell adhesion on the endothelial surface, prolong clotting time, and enhance the endothelial barrier function.

1.2.3 Functions of KLF4

1.2.3.1 Functions of KLF4 in vascular endothelial cells

It has been shown that elevated expression of KLF4 in cultured ECs under physiological conditions induces anti-inflammatory factors (eNOS) and anti-thrombotic factor (thromboxane (TM)) expression by inhibiting NF-κB activation(29). The deficiency of KLF4 activated harmful PH due to increased endothelin-1 and decreased eNOS. Likewise, lack of KLF4 enhances the expression of TNFα-induced VCAM-1 and tissue factor (TF)(30). The new study points out that in addition to maintaining anti-adhesion and anti-thrombotic endothelium, KLF4 also regulates EC autophagy gene expression(31). Overexpression of KLF4 in endothelial cells enhances autophagy and further protects the vascular network from

aging. Beyond that, KLF4 is known to induce VE-cadherin transcription in ECs, maintain normal endothelial barrier function, and prevent vascular leakage(32). Thus, KLF4 plays a significant protective role in vascular protection.

Furthermore, KLF4 suppresses angiogenesis and endothelial proliferation by increasing miR-15a in ECs and VSMCs(33). However, persistent expression of KLF4 causes impaired tumor growth by activating the Notch signaling pathway and promoting ineffective angiogenesis(34). Besides, *KLF4* also promotes angiogenesis by activating VEGF signaling(34). Thus, the regulation of angiogenesis by KLF4 may differ depending on the cell type and expression. During inflammation, the expression of TM and eNOS can be activated by overly expressed KLF4. *KLF4* acts as a decisive protective factor against thrombosis by inhibiting pro-thrombotic genes and activating anti-thrombotic genes. Overexpression of KL4 suppresses the expression of pro-inflammatory factors(35).

1.2.3.2 Functions of KLF4 in vascular smooth muscle cells

Vascular smooth muscle cells (VSMCs) play a central role in pathophysiology of vasculature(36). In a healthy adult organism, VSMCs are quiescent. However, according to vascular injury, they undergo a shift from contractile to synthetic, resulting in narrowing or occlusion of the vascular lumen. The transcription factor *Sp1* is a potent inhibitor of VSMC differentiation by upregulating the expression level of KLF4. Furthermore, the expression of KLF4 suppresses the expression of VSMC contraction mediators （such as SM α-actin, myocardia, and SM22-α). Hence, KLF4 is a crucial driver of VSMC phenotype switching(37).

1.2.3.3 Functions of KLF4 in tumors

By acting as an anti-proliferative factor expressed in the differentiated epithelium, *KLF4* may play two distinct roles as a tumor regulator or as a suppressor and oncogene(38). *KLF4* expression is widely decreased in various tumors. *KLF4* inhibits the expression of ornithine decarboxylase, which is a proto-oncogene(39). Accordingly, *KLF4* has tumor-suppressing properties. While *KLF4* may act as a tumor suppressor in various tissues, *KLF4* may also be an oncogenic gene. *KLF4* is involved in cell-cycle-arrest and differentiation. *KLF4* loss of function results in a lack of differentiation, thereby contributing to the emergence of pre-malignant lesions. *KLF4* transcription can either repress or activate *p53* expression(40). *p53* expression repression represents *KLF4* of the primary oncogenic function(40). In contrast, *KLF4* has also been placed downstream of the *p53* pathway and requires *p53*-mediated

induction of *CDKN1A* in response to DNA damage, which leads to cell cycle arrest. Thus, the tumor-regulating properties of *KLF4* are associated with *p53*.

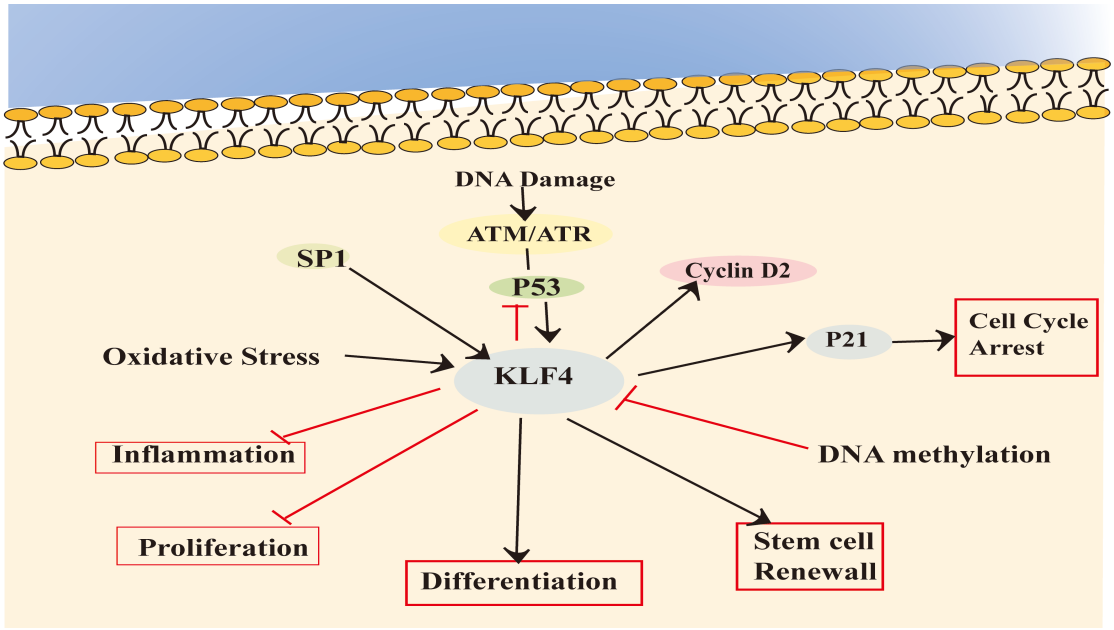

Figure 2. *KLF4* Signaling Pathway

KLF4 is a transcription factor with multiple functions. *KLF4* functions include anti-inflammation and anti-proliferation.

1.3 Gene therapy

1.3.1 AAV as a viral vector for gene therapy

Gene therapy is an innovative technique that uses the transfer of nucleic acid sequences to treat or prevent disease. Adeno-associated virus (AAVs) is a virus that is not known to cause human disorders. Therefore, AAV vectors are used for gene therapy(41). Other commonly used virus vectors are lentiviral vectors and adenoviral vectors(42).

Adeno-associated virus (AAVs) were first observed in the mid-1960s(43). With more in-depth research into AAVs' biological properties, the use of AAVs as gene delivery vectors has been promoted(44). Along with the understanding of virus-host interactions, AAVs are used as biotherapeutics. The life cycle of AAV depends on the presence of a helper virus, and it is found in various vertebrates, including humans and non-human primates. AAVs are currently considered safe and do not cause any human diseases.

The viral coding sequences must be ultimately maximally removed from the genomes encapsulated by recombinant AAVs in applications(44). This removal contributes to their low immunogenicity and cytotoxicity. The only sequence derived from viruses are two inverted

terminal repeat (ITRs), which guide genome replication and packaging during vector production. The optimal size of a therapeutic gene expression cassette designed in the AAVs genome should be 5.0 kb or less(45). Therefore, it is vital to consider the restorative transgene sequence and the regulatory elements necessary for gene expression (e.g., promoter and polyadenylation signal). As adeno-associated virus (AAV) vectors do not integrate into the genome and still enable a long-term gene expression in human cells, we have chosen to apply AAV vectors for endothelial gene transfer within this study.

1.3.2 Specificity of gene therapy

The specificity of gene therapy is another critical aspect. Effective de-targeting in rAAV genome design can minimize immunity of gene products(46). A tissue- or cell-type-specific promoter is used for de-targeting(41). The specification can also be increased by the inclusion of the 3′-untranslated region (UTR) of the miRNA-binding site for *miR-142-3p* to the vector cassette, which binds *miR-142-3p* abundant in antigen-presenting cells (APCs). That will effectively reduce the transgene expression in APCs, thereby reducing immunity to the transgene product(46). AAV-mediated transduction itself can be targeted by inserting distinct peptides in the vector surface. Previous experiments have shown that the peptide SLRSPPS exhibits high efficiency and low immunoreactivity for in situ transduction of human umbilical vein endothelial cells(47). The present investigation uses AAV serotype 9 vector with the targeting peptide SLRSPPS for in vitro studies and serotype 2 vector with the peptide ESGHGYF for gene transfer in lung arterial endothelial cells *in vivo*(48)

1.3.3 Translational application

Today, more than a dozen capsid serotypes are used as vectors in clinical trials, with the most popular AAV2-based platforms. However, newer, more efficient capsids, such as AAV8, AAV9, and AAVrh, are increasingly utilized in clinical trials. In most cases, a therapeutic strategy involves targeting a monogenic recessive disease through gene replacement. Fast-evolving gene-editing technology has offered a versatile toolbox for the direct repair of mutations in human diseases(49). A family of programmable nucleases has been developed to make DNA breaks, such as zinc-finger nucleases (ZFNs) and CRISPR-Cas-based editing(50)

1.3.4 Advantages of Adeno-associated viral vectors in gene therapy

AAV vectors are currently used in many gene therapy applications and have many benefits(46,51,52) .

1) Compared to other viral vectors, adeno-associated viral vectors (AAVs) are currently considered pathogenic(42,46,47).
2) Adeno-associated viruses (AAVs) do not insert into the genome and rarely alter the genomic structure; thus, they have a low oncogenic potential. In contrast to AAVs, either lentiviral or retroviral vectors will insert into the infected cells' genome and may alter the host genome structure. The insertion forms a stable genetic inheritance, and the result is potentially tumorigenic(49,51).
3) AAVs have low immunogenicity and cause a low inflammation reaction, thus enabling extended gene expression in the body. In contrast, adenoviral vectors have limited application prospects due to their high immunogenicity(46).
4) AAVs have a wide range of hosts and can transduce not only dividing cells but also quiescent cells. Besides, AAVs have more energetic targeting properties and can select specific organs for transduction(47,49).

2. Aims of the study

The primary goal of this project is to develop new gene therapy strategies to inhibit hypoxic pulmonary hypertension. In addition, this project should answer the following questions by clarifying the potential therapeutic value of a KLF4 gene transfer based on cellular experiments. In particular, the following questions should be answered:

1) Does AAV-mediated overexpression of KLF4 ameliorate the inflammatory response due to hypoxia?
2) Does AAV-mediated overexpression of KLF4 significantly maintain endothelial cell integrity and permeability due to hypoxia?
3) Does AAV-mediated overexpression of KLF4 potentially reverse endothelial to mesenchymal cell transformation due to hypoxia?
4) Does AAV-mediated overexpression of KLF4 improve mitochondrial dysfunction due to hypoxia?
5) How safe is it to use virus-mediated gene therapy to overexpress KLF4?

3. Materials

3.1 Hardware and supplies

3.1.1 Hardware

Designation	Source
Amersham™ Protran NC membrane	GE Healthcare
Axiovert 40 C Microscope	ZEISS
Cell Scraper 16cm 2-position blade	Sarstedt
Cellar cell culture dishes 6-, 12-well	Greiner Bio one
Centrifuge 5810	Eppendorf
CFX96 Real-Time PCR System	BioRad
Coverslips 18 mm diameter	Karl Hecht KG
Duomax 1030 horizontal rotator	Heidolph
Filter paper 110 mm diameter	Schleicher & Schuell
FluorChem Q Camera (Western Blot)	Alpha Innotech
Galaxy MiniStar Microcentrifuge	VWR
Heraeus Fresco 21 Centrifuge	Thermo Scientific
Heraeus Pico 21 Centrifuge	Thermo Scientific
Image J	National Institutes of Health
Infinite M200Pro microplate reader	Tecan
Magellan v.7.2	Tecan Life Sciences
Mini PROTEAN Tetra System	Bio-Rad
MyCycler Thermal Cycler	Bio-Rad
NanoDrop 2000 spectrophotometer	Thermo Fisher Scientific
Olympus BX53 microscope	MARIENFELD
Olympus DP72 camera	Olympus
Parafilm	Olympus
Pasteur pipettes, glass	BEMIS
Pipette tips Biosphere Filter Tip	ROTH
Pipette tips, with filter	Eppendorf Research
Pipettes 2 mL, 5 mL, 10 mL, 25 mL	Sarstedt
Pipettes Eppendorf-Reference	Sarstedt
Pipes	Hirschmann Laborgeräte
Power Pac HC	Bio-Rad
PP-Microplate 96-well	Greiner-Bio One

Precellys 24 homogenizer	IKA
qRT-PCR plates, 96-well, multiply	Sarstedt
RCT Basic magnetic stirrer	Sarstedt
Seven Easy pH-meter	Sarstedt
Slide 76x26x1 mm	Peqlab
SigmaPlot v.11.1	Systat Software Inc.
Stemi 2000-C microscope	Sarstedt
Steril-Cult 200 incubator	Mettler-Toledo
SterilGARD Hood	Zeiss
TE1502S precision scale	Labotect
Thermomixer Comfort	The Baker Company
Titan PCR-working station	Sartorius
Tubes 0.5 mL, 1.5 mL, 2 mL, 5 mL	Eppendorf
Tubes 15 ml, 50 ml	ScanLaf
Vacusafe ventilation	Integra Biosciences
Variomag Poly magnetic stirrer	Thermo Fisher Scientific
Vortex-Genie 2	Scientific Industries
ZEN v.2.3 (blue edition)	ZEISS

3.1.2 Chemicals

Designation	Source
Agarose	Biozym Scientific GmbH
Albumin fraction V, bovine	Merck KG
DAPI (4′,6-diamidino-2-phenylindole)	Sigma-Aldrich
DEPC (Diethyl pyrocarbonate)	Sigma-Aldrich
DMEM (Dulbecco's Modified Eagle Medium)	PAA Laboratories
DNA Loading Dye 6x	Fermentas
Collagen I – solution, bovine skin	BD Biosciences
DreamTaq 10x green buffer	Thermo Scientific
EDTA (Ethylenediaminetetraacetic acid)	Serva Electrophoresis
Ethanol	Carl Roth
Fluor Preserve Reagent	Calbiochem
Formamide	Sigma-Aldrich
iQ Powermix Reagent, multiplex qRT	Bio-Rad
Methanol	Carl Roth
PageRuler Plus prestained Protein Ladder	Thermo Fisher Scientific

Phenol/Chloroform/Isoamyl alcohol	Carl Roth
Protein-Assay dye-concentrate (Bradford)	Bio-Rad
QIAzol Lysis Reagent	Qiagen
Sodium chloride	AppliChem
Sodium hydroxide	AppliChem
SDS (Safety Data Sheet)	Serva Electrophoresis
TEMED 99% p.a. Electrophoresis	ROTH
Tris-Base	Carl Roth
Tris-HCl	Carl Roth
Triton X 100	Serva Electrophoresis
Tween 20	Sigma-Aldrich

3.2 Enzymes

Designation	Source
ECL-Select detection system	GE Healthcare
Platinum SYBR Green qPCR SuperMix	Invitrogen
Quick-RNA MicroPrep Kit	ZYMO Research
DC protein assay	Bio-Rad

3.3 Antibodies and Sequences of primers

Listed below are the primary and secondary antibodies used in this work for immunofluorescence (IF) and Western blot (WB). Some antibodies are coupled to fluorescent dyes (Fluorescein isothiocyanate (FITC), Alexa Flour (AF), Cyanine 5 (Cy5)), or horseradish peroxidase (HRP).

3.3.1 Primary Antibodies

Antibody	Species	Clonality	Company	Description
COX2	rabbit	poly	cell signaling	WB (1:1 000)
eNOS	mouse	mono	abcam	WB (1:1 000)
GAPDH	mouse	mono	Sigma	WB (1:10000)
ICAM-1	rabbit	poly	cell signaling	WB (1:1 000)
KLF4	rabbit	poly	abcam	WB (1:1 000)
MCP1	rat	mono	abcam	WB (1:1 000)
MMP9	rabbit	poly	abcam	WB (1:1 000)

PINK1	rabbit	poly	Novus bio	WB (1:1 000)
SOD2	rabbit	poly	cell signaling via NEB	WB (1:1 000)
ß-actin	mouse	mono	sigma	WB (1:10 000)
VCAM-1	rabbit	mono	abcam	WB (1:1 000)
VE-Cadherin	rabbit	poly	cell signaling	WB (1:1 000)
ZO-1	mouse	poly	Millipore	WB (1:1 000)
Mitofusin-2	rabbit	mono	abcam	WB (1:1 000)
CD31	rat	mono	Santa Cruz Biotechnology	IF (1: 200)
COX4	mouse	poly	abcam	IF (1: 400)
HIF1-α	rabbit	mono	Cell signaling	IF (1: 300)
Ki67	rabbit	mono	abcam	IF (1: 400)
KLF4	rabbit	poly	abcam	IF (1: 400)
Tom 20	mouse	poly	Santa Cruz Biotechnology	IF (1: 400)
ZO-1	mouse	poly	Millipore	IF (1: 400)
MitoSOX Red			Thermo Fisher scientific	IF (1: 100)

3.3.2 Secondary Antibodies

Antibody	Species	Clonality	Company	Description
mouse	goat	HRP	Santa Cruz	WB (1:10 000)
mouse	goat	AF546	Life Technologies	IF (1: 400)
mouse	goat	AF647	Life Technologies	IF (1: 400)
rabbit	goat	HRP	Santa Cruz	WB (1:10 000)
rabbit	goat	AF546	Life Technologies	IF (1: 400)
rabbit	goat	AF647	Life Technologies	IF (1: 400)
rabbit	goat	Cy3	Dianova	IF (1: 400)
rat	goat	HRP	Santa Cruz	WB (1:10 000)
rat	goat	Cy5	Dianova	IF (1: 400)

3.3.3 Sequences of the primers

Table 1. Quantitative real-time PCR primers

Name		Sequence (5'-3')
hKLF4	Fw:	CAAGAGCTCATGCCACCC
	Rv:	GTCCCAGTCACAGTGGTAAG
hCD31	Fw:	CTGCTGTCATTGCGCTGTGG

	Rv:	CATGTGGCCCCTCAGAAGACA
hvWF	Fw:	GCCTACGGCTTGCACCATTC
	Rv:	GCCATCCTGGAGCGTCTCAT
hVE-Cadherin	Fw:	AACATCCCTCAGCCCACAGG
	Rv:	ATCTCTCTTTTGGCGCCGGT
hTie2	Fw:	GGCCCAAGCCTTCCAAAACG
	Rv:	TGCGCGCCTTAAGAACTTGG
hSM22a	Fw:	GGAATTGATGGAAACCACCGGG
	Rv:	ACTTCGCGGCTCATGCCATA
hvimentin	Fw:	TCAATCGGCGGGACAGCAG
	Rv:	GACACGGACCTGGTGGACAT
hTNFα	Fw:	ACTTTGGAGTGATCGGCCCC
	Rv:	TGGGCTACAGGCTTGTCACT
hα-SMA	Fw:	GTCCCGGAGCAGGAGGATTC
	Rv:	GCATGCTTAAATGAAGCCACAGC
hTGF-β	Fw:	GATGTCACCGGAGTTGTGCG
	Rv:	GCCGGTAGTGAACCCGTTGAT
hMCP1	Fw:	AGAATCACCAGCAGCAAGTGTCC
	Rv:	TCCTGAACCCACTTCTGCTTGG
hMMP9	Fw:	GCCACTACTGTGCCTTTGAGTC
	Rv:	CCCTCAGAGAATCGCCAGTACT
hIL-6	Fw:	GGAAATGAGAAAAGAGTTGTGC
	Rv:	GTACTCCAGAAGACCAGAGG
hICAM-1	Fw:	TCCAGACCTTTGTCCTGCC
	Rv:	GTCGTTGCCATAGGTGACTG
hVCAM-1	Fw:	GAATGGGAAGGTGACGAATG
	Rv:	AGATTCACAAGTTGCTGTGC
mCdnk1A	Fw:	CACTTTGCCAGCAGAATAAAAGG
	Rv:	CCGTGACGAAGTCAAAGTTCC
mDnmt1	Fw:	TCTACTGCAGTTCCATCACC
	Rv:	GATCCTTCTTTGGGCGTTTC
mHSP90	Fw:	GTACTACTACTCGGCTTTCCC
	Rv:	CATTAGAGATCAACTCGCGG
mklf4	Fw:	CACCTGGCGAGTCTGACAT
	Rv:	AGAGAGTTCCTCACGCCAA
mp53	Fw:	AACTTACCAGGGCAACTATGG

	Rv:	TGGCAGAATAGCTTATTGAGGG
mp300	Fw:	GCCCAATGTGTCTAATGACC
	Rv:	TCAGGATCAACAATGGGAGG
mSV40p	Fw:	TGTTGTTGTTAACTTGTTTATTGCAGC
	Rv:	GATACATTGATGAGTTTGGACAAACC
mEGFP	Fw:	GCATCAAGGTGAACTTCAAGATCC
	Rv:	ATGTGATCGCGCTTCTCGTTG
mNOS3	Fw:	GAGCATACCCCCACTTCTG
	Rv:	CACACAGAAGGTTTCACAGG
mTjp1	Fw:	GAGACAAGATGTCCGCCAG
	Rv:	GGCCCTCCTTTTAACACATC

3.4 Kits

Designation	Source
ECL-Select detection system	GE Healthcare
Platinum SYBR Green qPCR SuperMix	Invitrogen
Quick-RNA MicroPrep Kit	ZYMOResearch
DC protein assay	Bio-Rad

3.5 Buffers and solutions

RIPA lysis buffer (pH 7.5)	50 mM Tris-HCL pH 7.5 titrate with 1 M NaOH 150 mM NaCl 0.5 % (w/v) Sodium Deoxycholate 1 % (v/v) NP-40 0.2 % SDS
Lysis buffer (1 ml)	40 µl 25x Proteinase-Inhibitor-Cocktail 10 µl Phosphatase-Inhibitor 2 10 µl Phosphatase-Inhibitor 3 1 µl 1 M DTT
Running buffer, SDS-PAGE (10x)	250 mM Tris 1.9 M Glycine 1 % (w/v) SDS

PBS	137 mM NaCl 2.7 mM KCl 4.3 mM Na_2HPO_4 1.47 mM KH_2PO_4, pH 7.4, autoclaved
PFA (2 bzw. 4%)	2 bzw. 4% (w/v) PFA in PBS
Laemmli buffer (4x)	250 mM Tris pH 6.8 5 % (w/v) SDS 40 % (v/v) Glycerin 0.005 % (w/v) Bromophenole blue 10 % (v/v) 2-Mercaptoethanol
Loading Buffer (for proterin) 4X	0.25M Tris-HCl pH 6.8 10% SDS 50% glycerol 0.5% bromphenol blue 0.8 M 2-mercaptoethanol 192 mM Glycine 0.037 % (w/v) SDS
Milk buffer (5%)	5% (w/v) milk powder in TBST
TBS-T	500 mM Tris-HCl pH 7.3 1.5 M NaCl 0.2% TWEEN 20

4. Methods

4.1 Cell culture

4.1.1 Culturing of immortalized HUVECs cell line

Primary human umbilical vein endothelial cells (HUVECs) were purchased from PromoCell (PromoCell GmbH, Germany) and cultured in Endothelial Cell Growth Medium (PromoCell GmbH, Germany). Immortalized cryo-conserved HUVECs were stored in big liquid nitrogen chambers. For culturing, cells were thawed rapidly in a 37 °C water bath and added with a 1 ml pre-warmed growth medium. This cell solution was transferred into a T75 cell culture flask containing 8 ml of warm growth medium. After 36 h for generation, all experimenters were conducted between passages 2 and 6 at a confluence of 70–80 %. Cells were dissociated from the plastic surface by adding 2 ml Trypsin-EDTA solution and incubated for 1-2 min at 37 °C until single cells were visible under the microscope. 10 ml of growth medium was added to the cell-solution to stop the trypsin activity. The cells were then centrifuged at 1 000 g at RT for 5 min. The supernatant consisting of Trypsin and media was discarded, and the cells were resuspended in a warm growth medium. The cells were counted in a Neubauer chamber and seeded in the respective culture plates or, without counting, plated at a ratio of 1:10 into new T175 flasks for maintenance of the cell line. All cell culture operations, like cell splitting and seeding, were performed under the sterile hood. Cells were incubated in a 37 °C incubator with 5 % CO_2 until the next use (transduction).
The cell count per ml was calculated based on the following formula:

$$(\text{average cell number}) \times (\text{dilution factor}) \times 10^4$$

4.1.2 Transduction with AAVs vectors *in vitro*

HUVECs were transduced with AAV (serotype 9 SLRSPPS(47), and small-scale productions were performed with 10^4-10^5 vg/cell MOI (multiplicity of infection) on the third day after seeding. The corresponding AAV vector was amount calculated and added to a serum-free medium (e.g., 2 ml medium per well of a 6-well plate) and mixed gently. The complete growth medium was removed and replaced by the AAV/serum-free medium mixture. At last, cells were incubated under two different conditions (Normoxia incubator with 37°C, 20 % O_2, and hypoxia incubator with 37 °C, 1 % O_2) for 48 hours.

Table 2. Experiment-dependent numbers of cells and volumes in cell culture

Cell type	Plate type	Experiment	Cell/ ml	Medium/ volume
HUVECs	12-well plate with coverslips	Immunofluorescence	$3 \cdot 10^4$	1 ml
	6-well plate	RNA/protein isolation	$5.5 \cdot 10^4$	2 ml

4.2 Induction of hypoxia

To grow cells in hypoxia, an incubator that controlled oxygen by suppressing it with nitrogen and regulating CO_2 level and humidity at the same time was used (Thermo scientific). Briefly, cells were cultured in a 6/ 12-well plate at 1.0 % O_2 for specified periods. Control cells were maintained in normoxia in a 20 % O_2 incubator (Thermo Scientific).

4.3 AAVs vector productions

AAVs vector were produced by Angela Schulz (University Hospital Schleswig-Holstein Campus Kiel) in our group according to standard protocols(45).

4.4 Molecular biology methods

4.4.1 RNA isolation and qRT-PCR

Total RNA was isolated from HUVECs using an RNA lysis buffer following a protocol (Quick-RNA Microprep kit (ZYMO Research, USA)). To isolated RNA from murine lung tissue, Trizol was used (QIAzol; Qiagen). 1 µg of DNA-free total RNA was transcribed into cDNA using the first-strand cDNA synthesis kit (SuperScript III; ThermoFisher Scientific). The EXPRESS SYBR Green ER reagent (Life Technologies, Inc.) was used in a real-time PCR system (CFX96; Bio-Rad). All experiments were performed in duplicates or in triplicates and repeated three times.

4.4.2 RNA extraction from cultured cells

Total RNA was isolated from cultured cells using Quick-RNA Microprep kit (ZYMO Research, USA). Before starting, RNA wash buffer was prepared (48ml, concentrate R1051) by adding 192 ml 100 % ethanol. The lyophilized DNase I with 275 µl DNase/RNA-Free water were mixed well for the following steps.

After the incubation period, the liquid medium was removed and collected for ELISA assay. Cells were lysed in the well by adding 300 µl of RNA lysis buffer and incubated for 10 min at room temperature. Then, 1:1 volume of 100 % ethanol was added. Cells were flushed with a pipette's help, and the mixture was transferred to Zymo-Spin IC Column in a Collection tube (provided in the kit). The samples were centrifuged with 12 000 g for 30 seconds, and the flow-through was discarded. Every column with 400 µl RNA Wash Buffer was prewashed. To prepare the DNase I Reaction Mix: each sample was mixed with 5 µl DNase I and 35 µl DNA Digestion Buffer. The DNase I Reaction Mix was added directly and incubated at room temperature for 15 min. Trace DNA was removed during this step. During the incubation time, new RNase-free tubes were prepared for RNA collection. After 15 min incubation, 400 µl RNA Prep Buffer was added to the column. Samples were centrifuged for 30 seconds, and the flow-through was discarded. 700 µl RNA Wash Buffer was added, and the flow-through was discarded after centrifugation. 400 µl RNA Wash Buffer was added to each column. For ensuring complete removal of the RNA Wash Buffer, the columns were centrifuged for 2 min at 12 000 g. The columns were carefully transferred into new RNase-free tubes, which were prepared during trace DNA removal processes. Finally, 15 µl DNase/RNA-Free water was added to the column matrix and centrifuged for 30 seconds at 12 000 g. Then the eluted RNA was collected in the flow-through and was readied to be measured by NanoDrop spectrometer. Then, RNA was stored at -80 °C until cDNA synthesis.

4.4.3 RNA isolation from murine lung tissue

For isolating total RNA from murine lungs, the tissue was broken beforehand by using the Precellys 24 homogenizer. Each tissue was placed in 2 ml tight capped tubes, and 1 ml Trizol lysis buffer with big (2.8 mm) and small (1.4 mm) ceramic beads were added. The homogenizer was programed two times for 20 seconds at speed 5000 g until complete dissociation of the tissue. The dissociated tissue lysing liquid was then centrifuged at 12 000 g for 20 min at 4 °C. The supernatant containing nucleic acids was transferred into a fresh 1.5 ml reaction tube. 200 µl Chloroform was added and mixed well by shaking. Samples were incubated at RT for 2 min and then centrifuged at 12 000 g for 15 min at 4 °C. The supernatant was transferred carefully to a new RNase and DNase free reaction tube. 500 µl isopropanol was added and mixed well for inducing RNA precipitation. Samples were incubated at -20 °C. After two hours of incubation, samples were centrifuged at 12 000 g for 10 min at 4 °C. Then, the supernatant was discarded, 1 ml 75% ethanol was added. After that, the samples were

further centrifuged at 7500 g for 5 min, and the supernatant was carefully discarded. The RNA-pellet was dried in an open reaction tube at room temperature by keeping tubes upside down for 10 min. 50 µl DEPC treated water was added and the concentration of the isolated RNA was determined by using NanoDrop at a wavelength of 260 nm. New DNA-free tubes were prepared for eluting RNA. 5 µl DNase I and 5 µl DNase buffer were added to each 5 ug RNA. DEPC treated water was added to achieve 100 µl volume in each tube. 1 µg of the isolated RNA was used for cDNA synthesis, and the rest was stored at -80 °C.

4.4.4 cDNA synthesis

For the transcription of the isolated RNA into cDNA, 1 µg RNA was added to 12 µl RNase-free water and mixed with 1 µl dNTPs (10 mM each) and 0.5 µl Random Hexamer Primer (50-250 ng). The mixture was incubated for 5 min at 65 °C, then transferred on ice for 1 min to avoid renaturation. For the transcription of RNA into cDNA, 6.5 µl Master Mix (Table 3.) was added to each of these preparations.

The transcription of mRNA into cDNA was performed in the Thermal Personal Cycler (see Table 4). For the annealing of the primer, the mix was incubated for 10 min at 25 °C. Afterward, the elongation step was performed at 50 °C for 60 min, followed by enzyme inactivation at 70 °C for 15 min. Finally, the reaction was stopped at 4 °C, and RNase-free water was added to the cDNA to obtain a concentration of 10 ng/ µl. The obtained cDNA was stored at -20 °C until further use.

Table 3. Master mix for the cDNA synthesis preparation

Component	Volume [µl]	Final concentration in the total volume of 20 µl
5x First Strand RT-Buffer	4	5 mM
DTT (0.1 M)	1	5 mM
RNase OUT (40 U/µl)	1	20 U/µl
SuperScript^{TM}III RT (200 U/µl)	0.5	20 U/µl
Σ	6.5	

Table 4. cDNA synthesis conditions

Step	Temp.	Time	Purpose
1	25 °C	10 min	Primer binding
2	50 °C	60 min	Enzyme activation, DNA synthesis
3	70 °C	15 min	Enzyme inhibition
4	4 ° C	∞	Cooling down, only after the last cycle

4.4.5 Gene expression determined by quantitative real-time PCR

The mRNA expression levels of various target genes and the housekeeping gene were quantified by the comparative ΔΔCt method. This method assumes an approximately equal efficiency of the PCR reactions of target and reference genes. The efficiency of the primers used was determined in preliminary tests using a cDNA dilution series. Gene expression determination of the target genes by quantitative real-time PCR was performed using the Express Sybr® GreenERTM qPCR SuperMix. The Platinum SYBR Green qPCR SuperMix (Thermo Fisher Scientific) was used to quantify gene copies. SYBR Green, a DNA-binding fluorescent dye, was detected and measured by PCR-cyclers. The expression of SYBR Green was enhanced with increasing DNA concentration. The primers were designed to span exon-exon junctions wherever possible to avoid amplifying possible contamination from genomic DNA during amplification. For the quantification, a reaction volume of 20 µl was used.
Technical triplicates were performed for each target gene. 18 µl of the master mix was added to a 96-well plate, 5 µl (*in vitro*) or 2 µl (*in vivo*) of cDNA was pipetted to the respective well. After sealing the plate with an adhesive foil, the plate was briefly spun down for 30 s at 2 000 g. Quantitative real-time PCR was performed using the following cycling conditions (CFX96TM Real-Time System).
The qRT-PCR data were analyzed using Microsoft Office Excel. The formula ΔCt (experimental gene) = Cq (experimental gene)-Cq (reference gene) was used to get the normalized Cq value. Next, the Cq value of a control sample was used to calculate ΔΔCt =ΔCt (experimental)- ΔCq(control). The value of $2^{-\Delta Ct}$ was calculated to reflect the expression fold change of the interest gene in every sample.

Table 5. Composition of each qPCR reaction (*in vitro*)

Component	Volume [µl]	Final concentration in total volume per well
Express Sybr® GreenERTM SuperMix	10	1x
Primer forward (10 µM)	1	0.5 µM
Primer reverse (10 µM)	1	0.5 µM
DNase-free water	3	-
Σ	15	

Table 6. Composition of each qPCR reaction (*in vivo*)

Component	Volume [µl]	Final concentration in total volume per well
Express Sybr® GreenERTM SuperMix	10	1x
Primer forward (10 µM)	0.4	0.2 µM
Primer reverse (10 µM)	0.4	0.2 µM
DNase-free water	3	-
Σ	18	

Table 7. qPCR cycling conditions

Reaction	Temperature	Time	Repeats
Initial denaturation	95 °C	3 min	1
Denaturation	95 °C	15 sec	39
Primer annealing and extension	60 °C	45 sec	

4.5 Protein isolation and Western blot experiments

4.5.1 Protein extraction from cultured cells

Post-incubation, HUVECs were washed once with ice-cold PBS before adding RIPA lysis buffer containing protease and phosphatase inhibitor cocktails (Roche Applied Science). Supernatants from each sample were collected and stored at -80 °C for future ELISA assay analysis. The lysis buffer mixture (600 µl) was prepared, as indicated below.

Table 8. Protease and phosphatase inhibitor cocktail for protein isolation

Component	Volume [µl]
RIPA Buffer	1000
Phosphatase inhibitor II	10
Phosphatase inhibitor III	10
Phosphatase inhibitor-cocktail 25X	40
DTT (1M)	1

Plates containing both cells and lysis buffer were frozen at -80 °C for half an hour to accelerate membrane lysis. After thawing on ice, the cells were scraped off with a cell scraper and transferred into a reaction tube. All the samples were ultrasonicated in an ice bath (Sonopuls GM 70, Bandelin) for 1 minute to disrupt cell membranes. The cell lysate was then centrifuged at 12 000 g for 10 min at 4 °C, and the supernatant was carefully transferred to a fresh reaction tube without disturbing the pelleted cell-debris. The samples were used to measure protein concentration (DC™-Protein concentration measurement assay) or were stored at -80 °C.

4.5.2 Protein extraction from murine lung tissue

Mouse lung tissues were collected in 2 ml tight capped tubes with big (2.8 mm) and small (1.4 mm) ceramic beads and stored at -80 °C. Samples were placed on ice, and 600 µl RIPA (with 1 % SDS) lysis buffer containing protease and phosphatase inhibitor cocktails was quickly added to each sample (Table 8.). For grinding solid tissue, the Precellys 24 homogenizer was used two times for 30 seconds at a speed of 5000 g until complete dissociation of the tissue. The dissociated tissues were centrifuged at 12 000 g for 20 min at 4 °C, and the supernatant was carefully transferred to a new tube. Each sample was diluted 1:10 (in RIPA buffer with 1 % SDS). The diluted samples were prepared for the DC assay measurement. All the samples were stored at -80 °C.

4.5.3 Protein concentration measurement using DC protein-assay kit

As mentioned above, the DC Protein assay kit (Bio-Rad) was used to determine the protein concentration from a cell lysate. A standard curve with a known protein concentration is necessary for analyzing the concentration of a given protein sample. A stock solution of 2 mg/ ml BSA was dissolved in the respective lysis buffer serially diluted four times to obtain standard dilutions from 2 mg/ ml to 0.125 mg/ ml in 20 µl of lysis buffer. The cellular protein

mix was also diluted using lysis buffer. The stock dilutions and protein dilutions were added in a quantity of 5 µl to each well in triplicates. Followed by the addition of 25 µl of solution A' (mixture ratio of solution A and solution S is 50:1) and 200 µl of solution B. The 96-well plate was gently mixed on a plate shaker for 1-2 min, then kept at room temperature for incubation about 15 min. The absorbances were stable for about 1 hour. A photometer TECAN M 2 000 pro, which was set for measurement of the OD at 750 nm, was used. The samples were measured photometrically, and the sample protein concentration was determinate using a BSA standard. Protein samples were prepared for loading and consisted of protein (20 µg), 4x Lämmli loading dye, and water. The samples were incubated at 95 °C for 5 min on a shaker. Then samples were stored at -80 °C.

4.5.4 SDS polyacrylamide gel electrophoresis (SDS-PAGE)

Sodium-dodecyl-sulfate (SDS) polyacrylamide gel electrophoresis (PAGE) was used to separate proteins with different molecular weights. Separating gel allowed the proteins to travel in the same direction and separated from one to another. At the same time, TEMED and APS (10 %) were added to induce polymerization. The mixture was vortexed well and the solution was filled into the cassette to about 80 % height. Isopropanol was immediately filled on top to remove any air bubbles. The separate gel was coagulated after 30 min. Isopropanol was discarded, and 4 % polyacrylamide collecting gel was poured on the top. A comb with 10 or 15 pockets was gently inserted in the collecting gel. After polymerization, the gel-chamber was set up.

The comb was removed, and gel pockets were washed with water. Then, the gel was placed into the chamber for electrophoresis and filled up with running buffer. The pockets were then loaded with samples. A pre-stained protein was used as a marker for molecular protein weights (PageRuler Plus, ThermoFisher). The electrical field was applied at a constant voltage of 80 V at the beginning until the marker was separated. 100 V was used until the loading dye reached the bottom of the gel-cassette.

4.5.5 Transfer the protein to PVDF membranes

A tank-transfer blotting chamber was used for transformation. During the transfer, proteins were transferred from polyacrylamide gel to a PVDF (polyvinylidene difluoride) membrane. The PVDF membrane was pre-activated with ethanol for 2 min. The SDS-gel, containing the separated proteins, was carefully taken out of the cassette and gently moved in the so-called "

blotting sandwich ". The " blotting sandwich" was fixed together in the following order: a sponge, three cellulose filter papers, the SDS-gel, an activated PVED membrane, three cellulose filter papers, and the other sponge. Any air-bubbles along the membrane surface were efficiently removed for the high quality of the transfer. The sandwich-containing cassettes were placed into the tank-transfer blotting chambers that were filled up with cold transfer buffer. The cold ice-packs were used for cooling down the whole transfer process. An electrical field was then applied at a constant 3 500 mA for 90-120 min (depended on the target protein's molecular weight). The pre-stained protein ladder was quickly found after blotting on the white membrane. The membrane with the size-separated proteins was then placed in a blocking buffer for 1-2 h at room temperature. The blocking buffer was commonly used as 5 % (w/v) dry-milk powder solved in TBS-T buffer or 5 % (w/v) BSA solved in TBST.

4.5.6 Detection of specific proteins

After blocking, the primary protein-specific antibodies were recognized and bound the specific protein on the membrane (diluted in the blocking buffer). The membrane was incubated overnight at 4 °C under rotation. The next day, the membranes were washed three times for 10 min in TBS-T buffer. Then, a suitable HRP-coupled secondary antibody (1:10 000 diluted in the blocking buffer; Santa Cruz Biotechnology) was added and incubated for 1hour at room temperature. After three times washing the membranes with TBS-T for 10 min at room temperature, the membranes were progressed to image. The Enhanced-chemiluminescence (ECL, Bio-Rad) detection was used. The ECL solutions were mixed in a 1:1 ratio, pipetted onto the membrane, and incubated for ~3 min in the dark. The membrane was then placed into the detection chamber of the Gel doc. The emitted chemiluminescence was detected using FluorChem Q software. According to the intensity of chemiluminescence, the exposure time was adjusted. The images were quantified by the Image J software (National Institutes of Health).

4.6 Immune staining

4.6.1 Immunofluorescence

Based on microscopic visualization, immunofluorescence staining was performed on HUVEC cells. As described above (Table 2.), HUVECs were prepared and plated in a 12-well plate on collagen-coated coverslips (1.5×10^6 cells/ well). Following AAV-mediated gene transfer (EGFP/KLF4 with a MOI of 5×10^{10} vg/ cell) and a 48 hours hypoxia-incubation phase,

coverslips were washed once with 1x PBS (1ml/ well). For fixation, cells were fixed with 4 % paraformaldehyde (PFA) for 5 min and blocked with PBS containing 2.5 % BSA and 0.1 % Triton X-100 (500 µl/ well) for 1 h at room temperature. Samples were incubated overnight at 4 ℃ with primary antibodies. The secondary antibodies were incubated for 1 h at room temperature. DAPI was used as a nuclear counterstain with a 1: 1 000 dilution. Up to 10 images from each coverslip was obtained by Keyence BZ-9000 microscope with 20x magnification. Cell-number counting and analysis were done by Image J software. Confocal images were captured with a Zeiss LSM800 laser-scanning microscope with 60x/0.8 oil objective.

4.6.2 Immunohistochemistry

Deparaffinization and rehydration was the first step for murine lung samples' affinization. The slides were immersed in three wells, one by one with Xylene, for 5 min. The slides were changed into two wells with 10% Ethanol and kept in each well for 10 min. After that, the slides were washed two times with fresh 95% Ethanol well for 10 min. Then the slides were gradually transferred into 70% Ethanol and infiltrated two times for 10 min. A brief wash in 1X PBS was the last step. The slides were incubated (0.1 % Triton X-100 and 2.5 % BSA in PBS) for 2 hours at room temperature. The primary antibody was diluted in blocking buffer and incubated at 4 ℃ overnight. Three times washing with 1X PBS was used, and the second antibody was incubated for 1 h at room temperature. DAPI was used as a nuclear counterstain with a 1: 1 000 dilution. Images were captured with a Zeiss LSM 800 laser-scanning microscope.

4.7 *In vivo* approaches

4.7.1 Animal models

All animals used in this thesis were kept under the supervision of the Animal Facility of University Hospital Schleswig-Holstein Campus Kiel. Animal care and use were conformed to the local animal welfare authorities (G124/ 13 Regierungspräsidium Karlsruhe, 12956/ 2018, MELUND Kiel, Germany). The mice were kept in IVC cages in a specified pathogen-free room, where the temperature (22 +/- 2 °C) and humidity (55 +/- 10 %) were controlled. A day/night rhythm was performed on 12/ 12 h. A complete diet and water were served ad libitum for the animals.

4.7.2 Tail vein injection

The mice were put into a restrainer and the tail was warmed in the water at 36 °C. Tail veins were localized, and AAV vectors were injected. Tail vein injections were performed by Susanne Hille (Molecular Cardiology, University Hospital Schleswig-Holstein Campus Kiel).

4.7.3 Virus efficiency test in mice

Eight-weeks old wild-type mice (C57BL/ 6J) were injected with AAV2- ESGHGYF (10^{12} viral particles/ mouse) virus in 0.1 ml PBS per mouse (eight mice of ssAAV2- ESGHGYF-ssCMV-EGFP group, eight mice of ssAAV2- ESGHGYF-ssCMV-Mm*Klf4* group, four mice of PBS were injected as a negative control group). For testing transgenes overexpressed efficiency, all mice were kept under normoxic conditions for five months. Afterward, the animals were killed, and organs were harvested according to the protocol and used for qPCR analysis.

4.8 Bioinformatics databases

4.8.1 ONCOMINE

ONCOMINE (www.oncomine.org). It is a platform for data mining by integrating data from the web. It is a systematic way to curate, analyze, and visualize data by pooling genetic annotation data from various genomic resources.
Data were collected to evaluate the expression of the *KLF* family in lung cancer. Data presented here, the significance thresholds were set as a *p* 0.05, a fold change of 2, and a gene rank in the top 10 %. The Student's *t*-test was used to analyze the difference in the expression of *KLF* family genes in non-small cell lung carcinoma.

4.8.2 GEPIA

GEPIA (http://gepia.cancer-pku.cn/index.html). GEPIA is a new web server for analyzing the RNA sequencing expression data of tumors and normal samples from the TCGA and the GTEx projects developed by Tang, Z. *et al.* in 2017.
In this study, a analysis of *KLF* expression was performed on the differential expression level between tumor and normal, profiling samples including cancer types or pathological stages, and patient survival. The *p*-value was 0.05, and a Student's *t*-test was used.

4.8.3 DAVID 6.8

DAVID 6.8 (https://david.ncifcrf.gov/home.jsp). DAVID is a biological knowledge base and analysis tool for systematically extracting bioinformatic resources from large gene/protein lists. Data mining techniques are used to visualize target genes' functional classification, functional annotation maps, or clustering and functional annotation tables.
From this database, Gene Ontology (GO) enrichment analysis and Kyoto Encyclopedia of Genes and Genomes (KEGG) pathway enrichment analysis of *KLF4* were collected. The *KLF4* closely up/downstream related genes were analyzed as well. In this study, the *p*-value cut-off point was 0.05. The GO enrichment analysis included: Biological processes (BP), cellular components (CC), and molecular function (MF).

4.8.4 TIMER 2.0

TIMER 2.0 (http://timer.comp-genomics.org). TIMER is a systematic resource for the comprehensive analysis of immune infiltration in different cancer types.
This study evaluated the correlation between KLF4 expression and immune cells' infiltration in non-small cell lung cancer. "Survival module" was used to evaluate the correlation among KLF4 expression level and clinical outcome in non-small cell lung carcinoma.

4.9 Statistical Analysis

For statistics, all results were shown as the mean ± SD. Statistical analyses of the data were performed using the two-tailed Student's *t*-test and two-way analysis of variance (ANOVA) followed by Student-Newman-Keuls applied. p-values < 0.01 were deemed statistically significant. All statistical data were performed with GraphPad Prism software.

5. Results

5.1 *In vitro*

5.1.1 Validation for the efficiency of AAV overexpression vector

For testing the transduction efficiency of adeno-associated viral overexpressed vectors, HUVECs were transduced with AAV9-SLRSPPS-ssCMV-EGFP and AAV9-SLRSPPS-ssCMV-Mm*Klf4* (1.5×10^6 cells/well) with a MOI of 5×10^{10} vg/cell. Transgene overexpression was analyzed by western blot. As showed in Figure 3a and b, cells were transduced with AAV-KLF4 expressed 7.5 times KLF4 protein than the control vector group (AAV-EGFP).

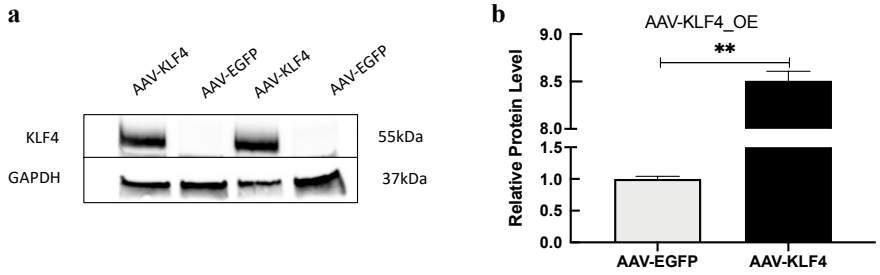

Figure 3. Validation for the efficiency of AAV overexpression vectors

HUVECs were transduced with AAV-KLF4, AAV-EGFP (1.5×106 cells/ well) with a MOI of 5×1010 vg/ cell. Every three wells of cells were transduced with one type of vector. Anti-GAPDH antibody was used as internal control 37 kDa (a and b). The relative level of KLF4 was analyzed with densitometry analysis. Statistical significance was determined using a Student's t-test. Error bars show mean ± SD. **, $p < 0.01$. OE, overexpression.

5.1.2 KLF4 overexpression inhibits pro-inflammatory response

Hypoxia-induced inflammation is widely recognized and generally accepted. Pro-inflammatory factors are activated in response to hypoxic stimuli and are involved in the overall inflammatory process. As KLF4 plays a central role in regulating vascular inflammation, the goal of this study was to evaluate the advantage of overexpressing KLF4 during hypoxia-induced changes. Hypoxia leads to endothelial dysfunction by releasing inflammatory mediators (intercellular adhesion molecule 1 (ICAM-1) and vascular cell adhesion molecule 1 (VCAM-1)). Pro-inflammatory phenotypes are activated by oxidative stress.

Upon low oxygen conditions, ICAM-1 is induced by IL-1 and TNF[9]. As shown in Figure 4a and b, in response to hypoxia, ICAM-1 protein was increased. The ICAM-1 protein level was

dramatically decreased in KLF4 groups, both under normoxia and hypoxia. These findings were also confirmed on the mRNA level (Figure 4c). VCAM-1 is a mediator of cell signals between leukocytes and endothelium. In response to cytokines, such as TNF-α and IL-1, VCAM-1 expression is up-regulated in endothelial cells. As a pro-inflammatory cytokine, the VCAM-1 expression on protein level was reduced in the KLF4 group, compared to the EGFP group (Figure 4d). However, there were no significant differences between normoxic and hypoxic groups (Figure 4e). Next, we tested *VCAM-1* on mRNA level was reduced in the KLF4 group, albeit without a significant difference between EGFP and KLF4 group in hypoxia (Figure 4f).

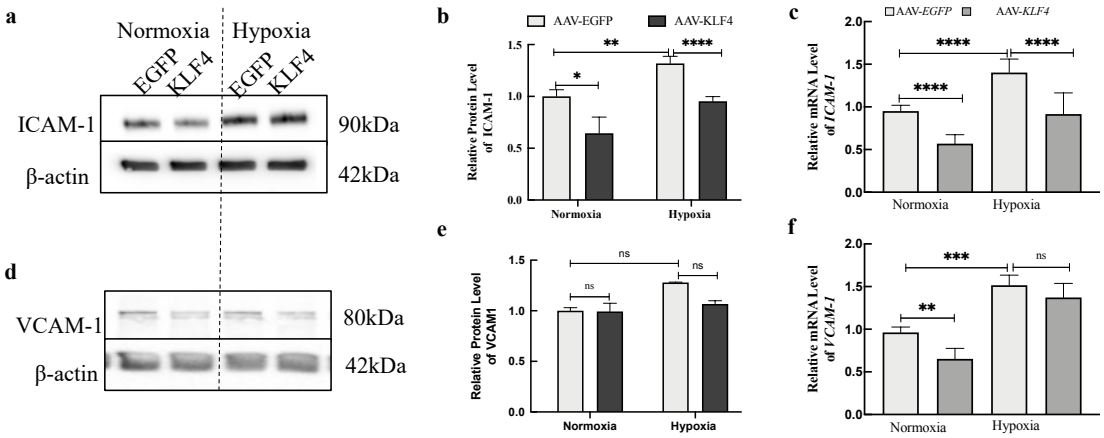

Figure 4. KLF4 overexpression inhibits pro-inflammatory response

HUVECs were transduced with AAVs and exposed to hypoxia for 48 hours. EGFP was used as a control to maintain an equal quantity of virus. Protein lysates were collected. (a and b) Quantification and statistical analysis of ICAM-1 expression on the protein level. (c) Quantification and statistical analysis of *ICAM-1* expression on the mRNA level. (d and e) Quantification and statistical analysis of VCAM-1 expression on the protein level. (f) Quantification and statistical analysis of *VCAM-1* expression on the mRNA level. Anti-ß-actin antibody was used as internal control 42 kDa. *RPLP0* was used as a housekeeping gene. Data are shown as mean ± SD of three independent experiments conducted in triplicates. Statistical significance was determined using One-way ANOVA Multiple Comparison (Student-Newman-Keuls method). *, $p < 0.05$; **, $p < 0.01$; ***, $p < 0.001$; ns, non-significant.

Nitric oxide (NO) is synthesized by endothelial NOS (eNOS) and secreted by vascular endothelium for maintaining vascular homeostasis[22]. Hypoxia-induced endothelial dysfunction results in less eNOS release, which causes a reduction of NO production. In this study, we verified that hypoxia resulted in downregulation of eNOS on protein levels in HUVECs. eNOS expression level was elevated by overexpression of KLF4 in either normoxia or hypoxia (Figure 5a and b). Cyclooxygenase-2 (COX2), as a pro-inflammatory agent, is repaired by activating prostaglandins[17]. Inhibition of COX2 has shown an anti-inflammatory

effect. The results we presented (Figure 5c and d) were consistent with this concept. Hypoxia-stimulation elevated levels of COX2, which was suppressed by overexpression of KLF4.

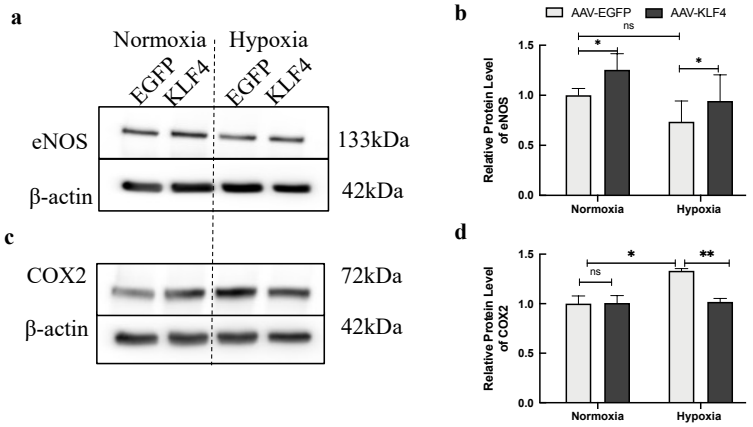

Figure 5. KLF4 overexpression inhibits inflammatory response

HUVECs infected with AAV-KLF4 and AAV-EGFP. HUVECs were exposed to hypoxia for 48 hours. (a and b) Quantification and statistical analysis of eNOS expression on the protein level. (a and b) Quantification and statistical analysis of COX2 expression on the protein level. (c and d) Anti-ß-actin antibody was used as internal control 42 kDa. Data are represented from three independent experiments conducted in triplicates. Statistical significance was determined using One-way ANOVA Multiple Comparison (Student-Newman-Keuls method). Error bars show mean ± SD *, $p < 0.05$; **, $p < 0.01$; ns, non-significant.

Matrix Metalloproteinase-9 (MMP9) indicates extracellular matrix remodeling and angiogenesis. MMP9 expression is triggered by vascular injury and increased secretion from SMCs following inflammatory stimuli. HUVECs showed an inflammatory response due to hypoxic exposure for 48 hours, which was reflected by a trend to higher levels of MMP9 protein in the hypoxic conditions (not significant). Overexpression of KLF4 showed a trend towards lower MMP9 levels (Figure 6a and b). Besides, hypoxia-impaired endothelial cells with KLF4 directly reduced the *MMP9* mRNA level identified on the protein level (Figure 6c). Monocyte chemoattractant protein 1 (MCP1) attracts monocytes into the site of active inflammation. Increased MCP1 levels indicates an ongoing inflammation. As expected, hypoxia elevated *MCP1* expression. Figure 6d shows a reduced in *MCP1* expression in the KLF4 group on mRNA level under hypoxia and also nomoxia.

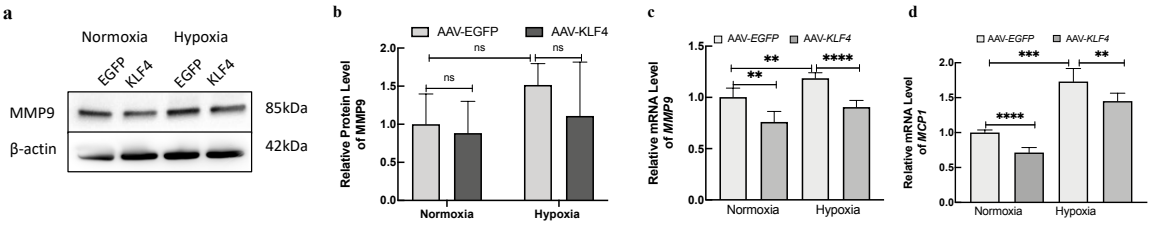

Figure 6. KLF4 overexpression plays an anti-inflammatory role under hypoxia

HUVECs infected with AAV-KLF4 and AAV-EGFP. HUVECs were exposed to hypoxia for 48 hours. (a and b) Quantification and statistical analysis of MMP9 expression on the protein level. (c and d) Quantification and statistical analysis of *MMP9* and *MCP1* expression on the mRNA level. Anti-ß-actin antibody was used as internal control 42 kDa. *RPLP0* was used as a housekeeping gene. Data are represented from three independent experiments conducted in triplicates. Statistical significance was determined using One-way ANOVA Multiple Comparison (Student-Newman-Keuls method). Error bars show mean ± SD, **, $p < 0.01$; $p < 0.001$; ****, $p < 0.0001$; ns, non-significant.

As stated above, hypoxia activates NF-κB and thus up-regulats the expression of various interleukins (ILs), including IL-1, IL-6, TGF-β, and TNF-α. IL-6, an oxygen-regulated protein, is synthesized and released from endothelial cells by exposure to hypoxia. In normoxia, KLF4 had no effect on *IL-6* expression and the expression of *TNF-α* in HUVECs. *IL-6* and *TNF-α* mRNA level were significantly reduced by KLF4 overexpression in hypoxia (Figure 7a and b). The consistent with the previous observation, *TGF-β* mRNA levels were significantly increased under hypoxia. KLF4 group showed a significant decrease in *TGF-β* mRNA levels under hypoxia (Figure 7c).

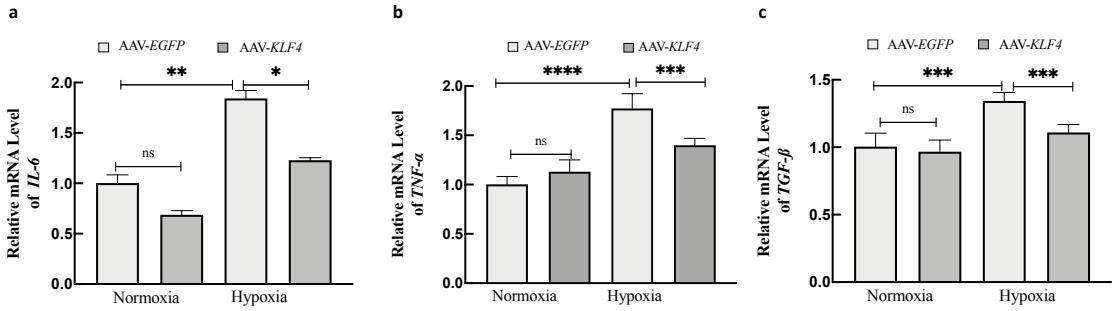

Figure 7. Cellular pro-inflammatory and procoagulant responses were inhibited

HUVECs were transduced with AAV-EGFP and AAV-KLF4, then cells were exposed to hypoxia for 48 hours. (a) *IL-6* mRNA levels were quantified by qRT-PCR. (b) *TNF-α* mRNA levels were quantified by qRT-PCR. (c) *TGF-β* mRNA levels were quantified by qRT-PCR. *RPLP0* was used as a housekeeping gene. Data are shown as mean ± SD of three independent experiments conducted in triplicates. Statistical significance was determined using One-way ANOVA Multiple Comparison (Student-Newman-Keuls method). *, $p < 0.05$; **, $p < 0.01$; ***, $p < 0.001$; ****, $p < 0.0001$; ns, non-significant.

Ki67 protein is used as a proliferation marker. In hypoxia, the kernel staining of Ki67 was significantly higher than that of the normoxia group. Ki67 expression level was markedly reduced by KLF4 overexpression (Figure 8a and b).

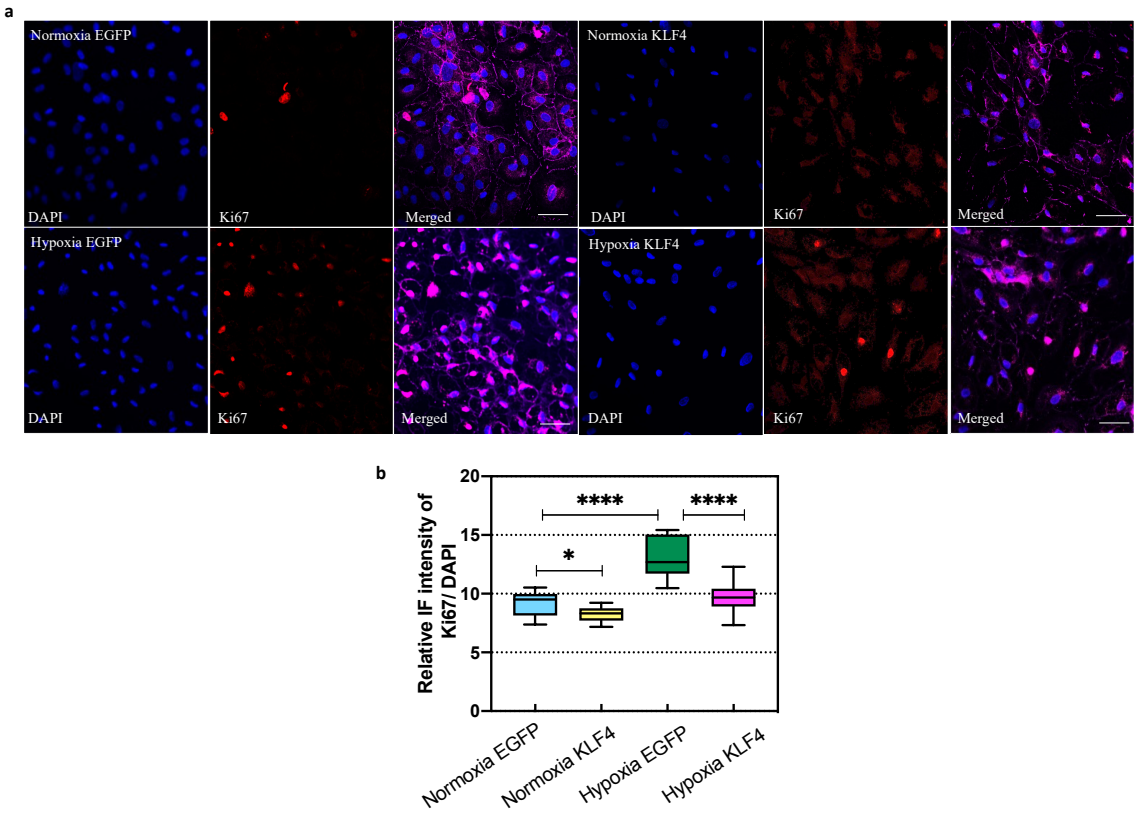

Figure 8. KLF4 overexpression suppresses cellular proliferation under hypoxia

(a) Representative confocal images of cells stained with anti-Ki67 antibody (red). HUVECs were transduced with AAV-KLF4/EGFP and were cultured on coverslips in triplicates at hypoxic conditions for 48 hours (lower lane); cells in normoxia were used as control (upper lane). Ki67 gene encoded a nuclear protein that was associated with cellular proliferation. Hypoxia increased Ki67 expression, but cells with KLF4 overexpression showed a reduced proliferation. DAPI (blue) was used as a nuclear counterstain. (b) Ki67 was represented from three independent experiments conducted in triplicates. Olympus BX53 microscope was used, and images were analyzed by Image J software. Scale bar (shown with a white line) represents 20 µm. Data are shown as mean ± SD. Statistical significance was determined using One-way ANOVA Multiple Comparison (Student-Newman-Keuls method). *, $p < 0.05$; ****, $p < 0.0001$; IF Immunofluorescence.

5.1.3 KLF4 overexpression efforts on reversing EndMT

5.1.3.1 Obstruct EndMT by overexpressing KLF4

Stimulation by external factors and changes in cell morphology occur during EndMT. Structural and functional remodeling of endothelial cells occurs during EndMT. Also, the cytoskeleton is rearranged and cell-cell adhesion is altered. Endothelial markers on mRNA levels (such as *CD31*, *Tie2*, *vWF*) were tested in this study. Compared to EGFP group, KLF4 group was significantly increased under hypoxia (Figure 9a-c). Besides, we also showed that mesenchymal phenotype markers, such as *vimentin*, *α-SMA*, *SM22α*, compared to EGFP group, were dramatically decreased in overexpression KLF4 group under hypoxia (Figure 9d-f).

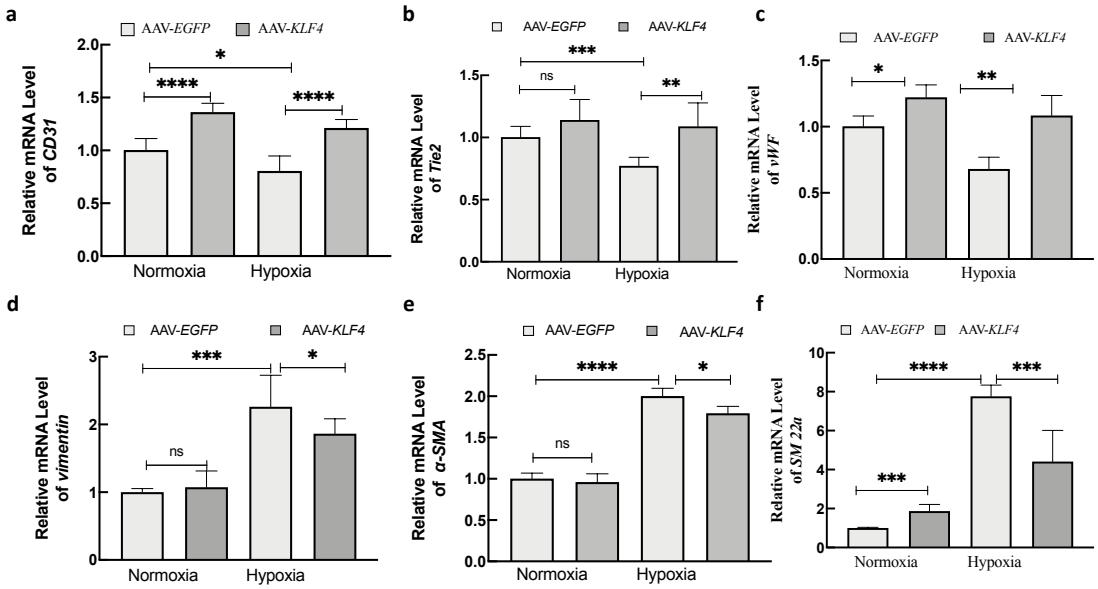

Figure 9. KLF4 overexpression is associated with reduced EndMT under hypoxia

HUVECs were transduced with AAVs and exposed to hypoxia for 48 hours. *EGFP* was used as a control. (a) *CD31* mRNA level was quantified by qRT-PCR. (b) *Tie2* mRNA level was quantified by qRT-PCR. (c) *vWF* mRNA level was quantified by qRT-PCR. (d) vimentin mRNA level was quantified by qRT-PCR. (e) α-SMA mRNA level was quantified by qRT-PCR. (f) SM22α mRNA level was quantified by qRT-PCR. *RPLP0* was used as a housekeeping gene. Data are shown as mean ± SD of three independent experiments conducted in triplicates. Statistical significance was determined using One-way ANOVA Multiple Comparison (Student-Newman-Keuls method). *, $p < 0.05$; **, $p < 0.01$; ****, $p < 0.0001$; ns, non-significant.

5.1.3.2 Preservation of cell-cell adhesion by overexpression of *KLF4*

Post-oxygen tension (hypoxia) affects endothelial cell physiology in a wide variety of ways. These effects include transcriptional regulation of the expression of vasoactive elements and matrix proteins. ZO-1 protein was located on the cytoplasmic membrane surface and contributed to the cell-cell tight junction. VE-cadherin is a critical element of endothelial cell-cell junctions, and maintain vascular integrity. The endothelial cell- cell junction was not significantly repaired by overexpression KLF4 on VE-Cadherin (Figure 10a and b) or on ZO-1 protein levels (Figure 10d and e). But Figure 10c illustrated that *VE-Cadherin* on mRNA level, was significantly increased by overexpression KLF4 under hypoxia. Figure 11a was visually presented a ZO-1 immunofluorescence staining plot. Image J software was used for quantifying the fluorescence intensity. KLF4 efforted on maintaining the integrity of intercellular connectivity under hypoxic conditions (Figure 11b).

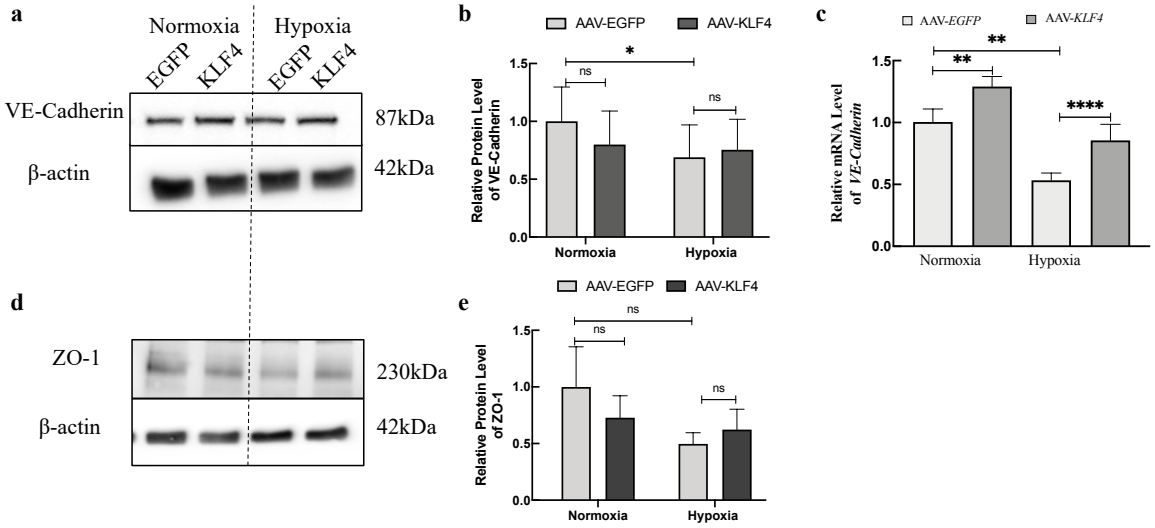

Figure 10. KLF4 overexpression supports the integrity of the endothelial barrier junction

HUVECs were transduced with AAVs and exposed under hypoxia for 48 h. EGFP was used as a control. Protein lysates and RNA were collected. (a and b) Quantification and statistical analysis of VE-Cadherin expression on the protein level. (c) *Ve-cadherin* mRNA level was quantified by qRT-PCR. *RPLP0* was used as a housekeeping gene. (d and e) Quantification and statistical analysis of ZO-1 expression on the protein level. Anti-ß-actin antibodies used as internal control 42 kDa. Data are shown as mean ± SD of three independent experiments conducted in triplicates. Statistical significance was determined using One-way ANOVA Multiple Comparison (Student-Newman-Keuls method). *, $p < 0.05$; **, $p < 0.01$; ****, $p < 0.0001$; ns, non-significant.

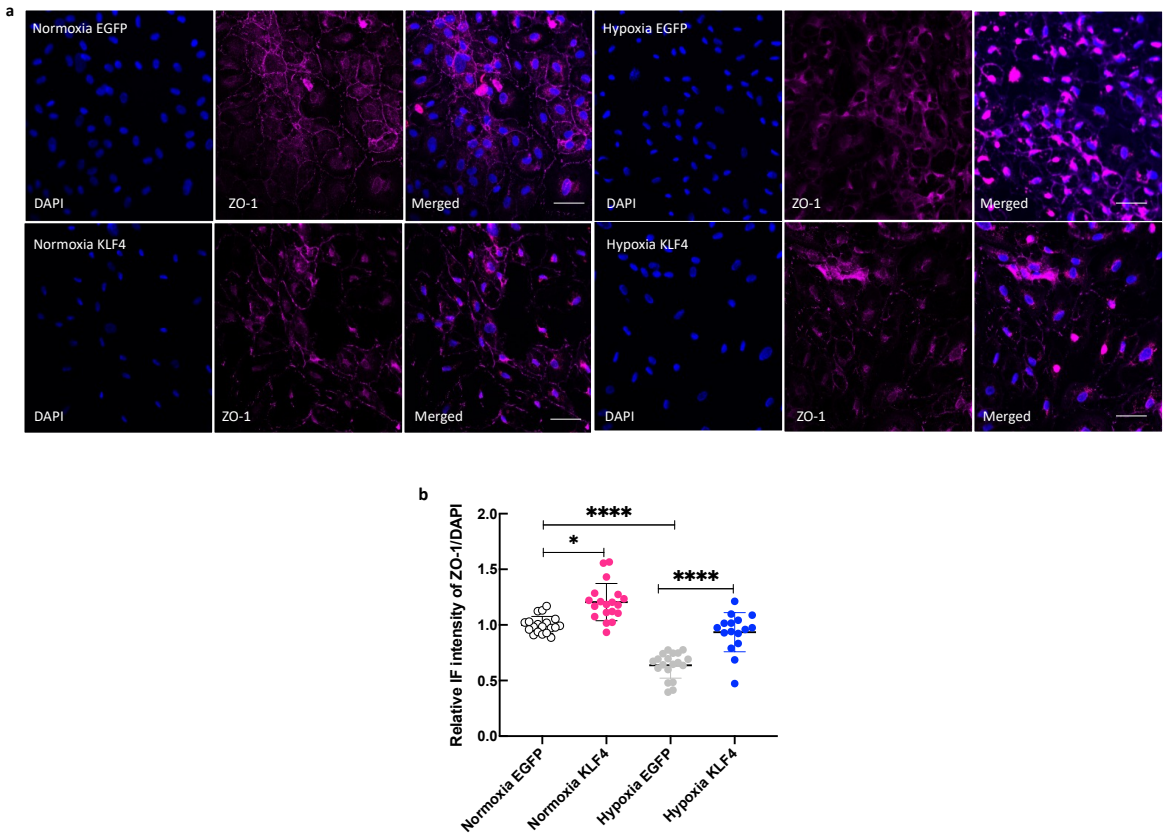

Figure 11. KLF4 overexpression protects cell-cell junction

(a) Confocal microscopy images were taken at 20x magnification. Cells were cultured under hypoxic conditions for 48 hours (lower lane) and stained with anti-ZO-1 antibody (red); cells in normoxia were used as control (upper lane). ZO-1 protein was located on the cytoplasmic membrane surface and contributed to the cell-cell tight junction. DAPI (blue) was used as a nuclear counterstain. Scale bar (shown with a white line) represents 100 µm. (b) ZO-1 was represented from three independent experiments conducted in triplicates and analyzed by Image J software. Data are shown as mean ± SD. Statistical significance was determined using One-way ANOVA Multiple Comparison (Student-Newman-Keuls method). *, $p < 0.05$; ****, $p < 0.0001$. IF, Immunofluorescence.

5.1.4 KLF overexpression preserves mitochondrial function

As we know, mitochondria are often referred to as the cell's powerhouse, providing the energy. PINK1 (PTEN-induced kinase 1) is processed and released from healthy mitochondria. Hypoxia caused mitochondrial dysfunction and hence reduced PINK1 expression. A trend to increased PINK1 under low oxygen conditions in the KLF4 group (Figure 12a and b) indicated that KLF4 overexpression may preserve mitochondrial function and reduce mitochondrial damage.

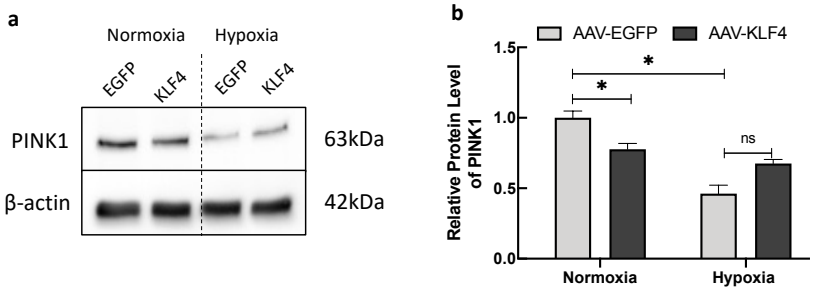

Figure 12. KLF4 overexpression improved Mitochondrial dysfunction

HUVECs were transduced with AAV-KLF4/EGFP and were exposed to hypoxia for 48 hours. (a and b) Quantification and statistical analysis of PINK1 expression on the protein level. Anti-ß-actin antibody was used as internal control 42 kDa. Data are shown as mean ± SD of three independent experiments conducted in triplicates. Statistical significance was determined using One-way ANOVA Multiple Comparison (Student-Newman-Keuls method). *, $p < 0.05$; ns, non-significant.

5.2 Establishment of KLF4 overexpression *in vivo*

5.2.1 Transduction efficiency of AAVs overexpression vector

Mice were random injected of AAVs vectors (10^{12} viral particles/mouse): AAV-*Klf4* (n=8), AAV-EGFP (n=8); PBS (n=4) was used as an additional control. Mouse left lung tissue RNA was collected five months after injection. For testing the efficiency of AAVs vectors *in vivo*, we isolated RNA from mouse lung tissue. We first confirmed that EGFP was significantly up-regulated compared with the other two groups (Figure 13a). However, mouse VVR4 was excluded cause of a significant outlier, which was tested by Grubb's test. (p=2.341). *SV40pA* is a primer that is used for detection of AAVs vector genomes. As shown in Figure 13b, EGFP and *Klf4* groups showed distinct, but variable amounts of AAV vector genomes compared to PBS controls. Nevertheless, there were no significant differences with statistical analyses. Taken together, we could detect significant EGFP mRNA expression, but not AAV vector genomes, most probably due to lacking sensitivity to detecting low levels of AAV vector genomes 5 months after injection.

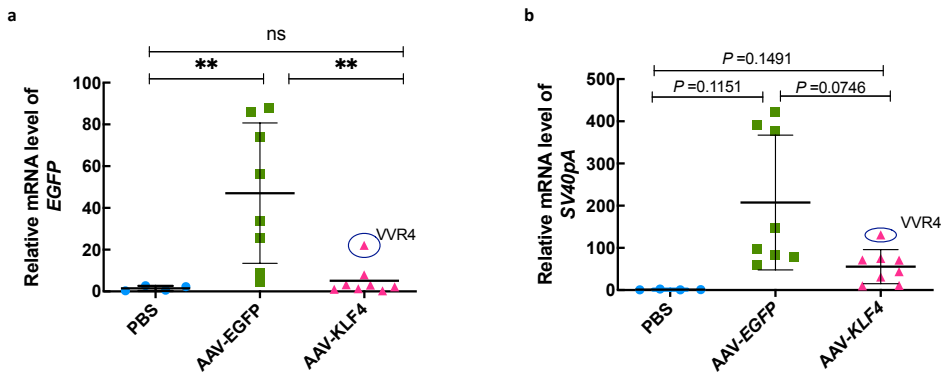

VVR4 was a significant outlier. Grubb's test. (p=2.341)

Figure 13. AAV vector transduction efficiency in mouse lungs

The efficiency of lung endothelial-specific AAV vectors. Mice were injected with AAV vectors, and the total RNA of lung tissue was collected. (a) *EGFP* mRNA levels were quantified by qRT-PCR. (b) *SV40pA* mRNA levels were quantified by qRT-PCR. *RPL32* was used as a housekeeping gene. Mouse VVR4 was a significant outlier as tested by Grubb's test. (p=2.341). Data are shown as mean ± SD. Statistical significance was determined using One-way ANOVA Multiple Comparison (Student-Newman-Keuls method). **, $p <$ 0.01, ns, non-significant.

5.2.2 AAV-*Klf4* overexpression after injection

After confirming the AAV vectors' efficiency, we analyzed the expression level of transgene *Klf4* on mRNA level. It was shown that *Klf4* groups presented to upregulation trend both in the left and right lungs. However, in contract to EGFP overexpression (Figure 13a), there was no statistical difference (Figure 14a and b).

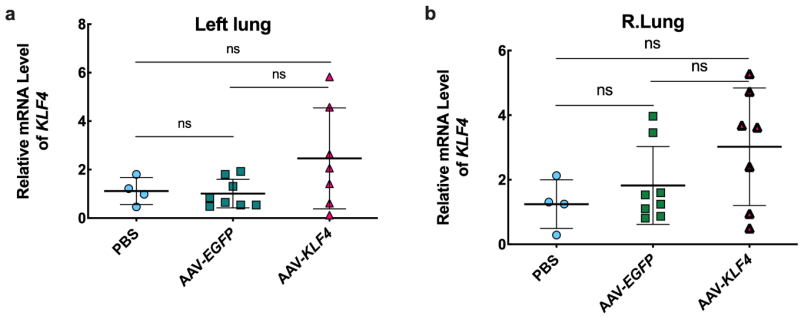

Figure 14. AAV-*Klf4* expression in murine model

The *Klf4* overexpression after injection. Mice were injected with AAV-*Klf4* (n=7), AAV- *EGFP* (n=8); PBS (n=4) was used as an additional control. Total RNA was collected. (a) Left lung *Klf4* mRNA levels were quantified by qRT-PCR. (b) Right lung *Klf4* mRNA levels were quantified by qRT-PCR. *RPL32* was used as a housekeeping gene. Data are shown as mean ± SD. Statistical significance was determined using One-way ANOVA Multiple Comparison (Student-Newman-Keuls method). ns, non-significant.

5.2.3 The role of overexpression *Klf4* gene in wide type mice

It should be studied whether in the case of overexpression of the *Klf4* gene, oncogenic genes, such as *p53*, *p21*, *p300,* are activated. Nevertheless, we chose and tested some genes which are down-stream of the *Klf4* gene for analysis of safety. *p53* is a critical oncogene that is closely related to *Klf*4 and regulates each other's expression levels. Figure 15a was showed that *p53* expression was not significantly altered. *Cdnk1* (*p21*) and *p300* are also down-stream genes of *Klf*4*,* which were regulated both by *Klf4* and *p53*. As shown in Figure 15b and c, overexpression of *Klf4* did not alter the expression levels of *p21* and *p300*. Unfortunately, however, these results were not statistically significant.

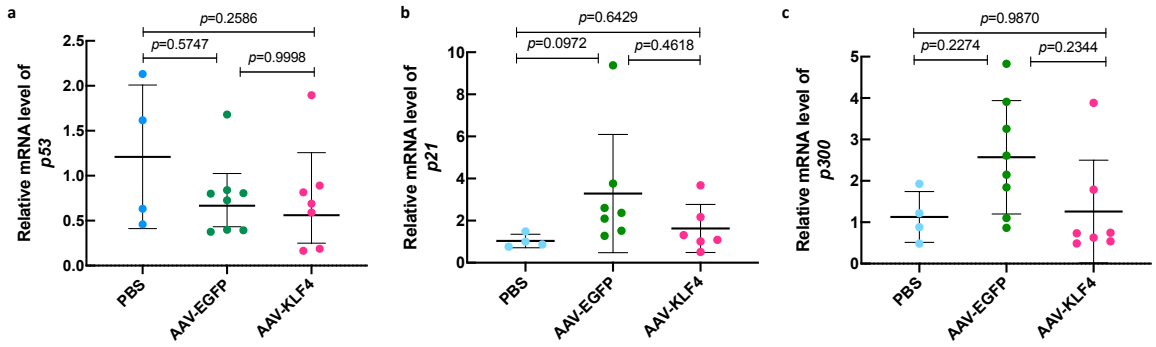

Figure 15. Expression of *Klf4* depended genes in mice injected with AAV-KLF4 /EGFP

Klf4 overexpression in wide type mice. Mice were injected with AAV-*Klf4* (n=7), AAV- *EGFP* (n=8); PBS (n=4) was used as an additional control. Total RNA was collected. (a) *p53* mRNA level was quantified by qRT-PCR. (b) *p21* mRNA level was quantified by qRT-PCR. (c) *p300* mRNA level was quantified by qRT-PCR. *RPL32* was used as a housekeeping gene. Data are shown as mean ± SD. Statistical significance was determined using One-way ANOVA Multiple Comparison (Student-Newman-Keuls method).

5.3 The bioinformatics of *KLF4*

5.3.1 Functional enrichment analysis

DAVID 6.8 and ONCOMINE were used to perform functional analysis of the *KLF4* gene. Figure 16a illustrates the top 10 most enriched GO items using DAVID. The ten most highly enriched functions in the biological process (BP) class, maintenance of stem cell numbers, negative regulation of macromolecules or cellular, regulation of RNA or cell differentiation are all associated with *KLF4* biological function. The transcription factor complex, the nuclear chromatin, the transcription factor complex, and the nuclear lumen were among others in the ten most highly enriched items in the cellular component (CC) category. In the molecular

function MF category, DNA binding transcription activities are identified. KEGG pathway analyses were performed and displayed in Figure 16b. Among the top 20 KEGG pathways, the Hippo signaling pathway, adherence junction, and the *TGF-beta* signaling pathway are involved in EndMT.

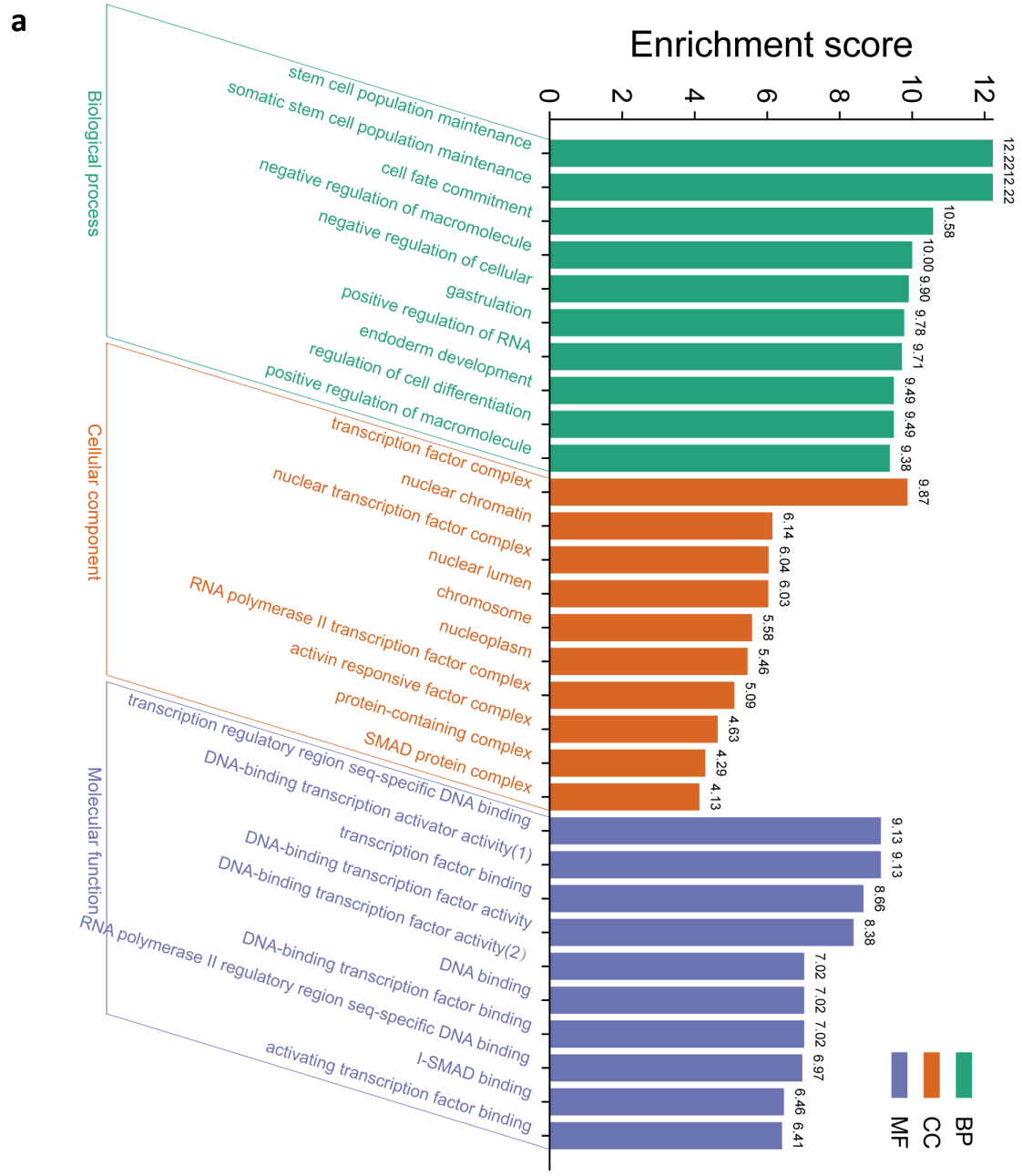

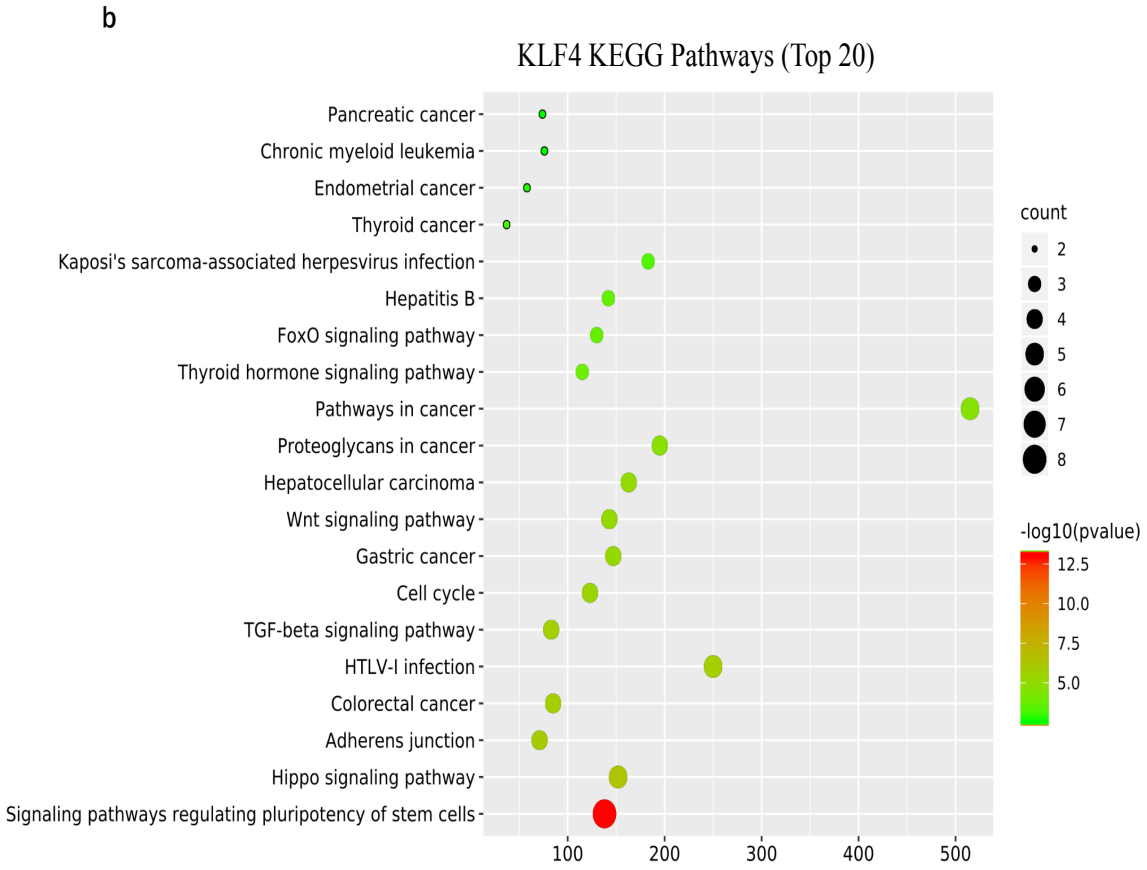

Figure 16. Functional enrichment analysis of the *KLF4* gene (David 6.8)

(a) GO enrichment in cellular component terms (CC), biological process terms (BP), and molecular function terms (MF) (Top 10). (b) Dotplot of *KLF4* KEGG enriched terms (Top 20).

5.3.2 The role of *KLF4* in non-small cells lung carcinoma

As indicated above, *KLF4* is involved in tumorigenesis and progression pathways. We performed a correlative bioinformatics analysis of *KLF4* gene expression to clarify the role of *KLF4* in the development and progression of non-small cell lung carcinoma.

To evaluate the differential *KLF4* expression, we assessed the correlation between normal and tumor tissues in different tumor types using GEPIA. From Figure 17a, it was shown that *KLF4* expression is lower in tumors compared with normal tissue, especially in non-small cells lung carcinoma (LUAD: Lung Adenocarcinoma; LUSC: Lung squamous cell carcinoma). Compared to *KLF* family expression in Figure 17b, we noticed that KLF4 expression in LUAD ($p< 0.05$) and LUSC were decreased in the tumor.

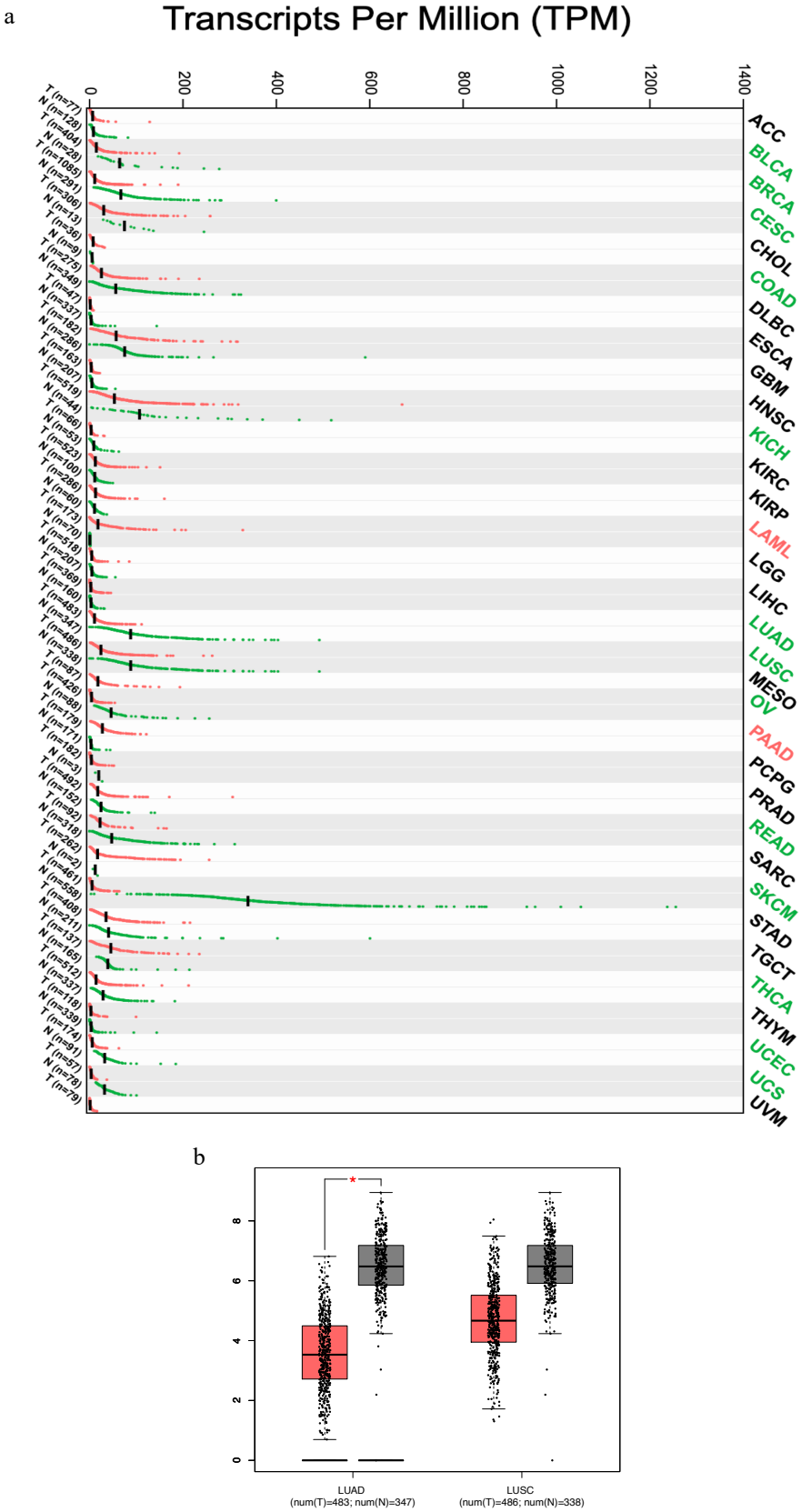

Figure 17. The *KLF4* expression in non-small cell lung carcinoma

(a) In all kinds of tumors, *KLF4* expression was decreased. (b) Box plot of non-small cells lung carcinoma, *KLF4* expression was significantly reduced. The *p* value was set at 0.05.

5.3.3 The correlation of *KLF4* gene with *p53* mutation

The relationship between the *KLF4* gene and the *p53* gene is complex, regulating each other's expression levels. *p53* mutation is one of the key changes in tumorigenesis and progression. Here, we showed the relationship between low expression of *KLF4* and *p53* mutation in LUAD and LUSC. Figure 18a and b indicated that *KLF4* expression presented a decreased trend in mutated *P53* groups, compared with wide type. Statistical analysis was determined using Wilcoxon, p=0.049 (Figure 18a), p=0.082 (Figure 18b).

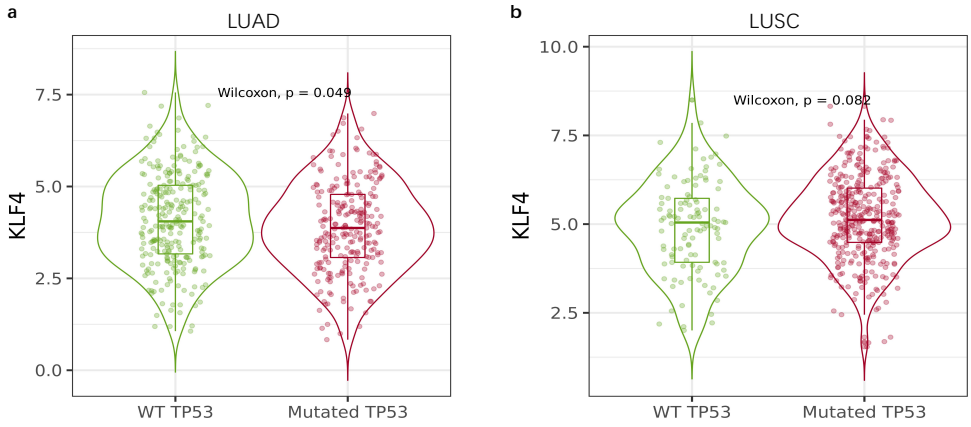

Figure 18. The correlation of the *KLF4* gene with *p53* mutation (GEPIA)

Compared to wide type, *KLF4* expression in mutated *P53* groups presented a decrease in LUAD and LUSC. Statistical analysis was determined using Wilcoxon, p=0.049 (a), p=0.082 (b).

5.3.4 The correlation between lung carcinoma survival and KLF4 expression levels

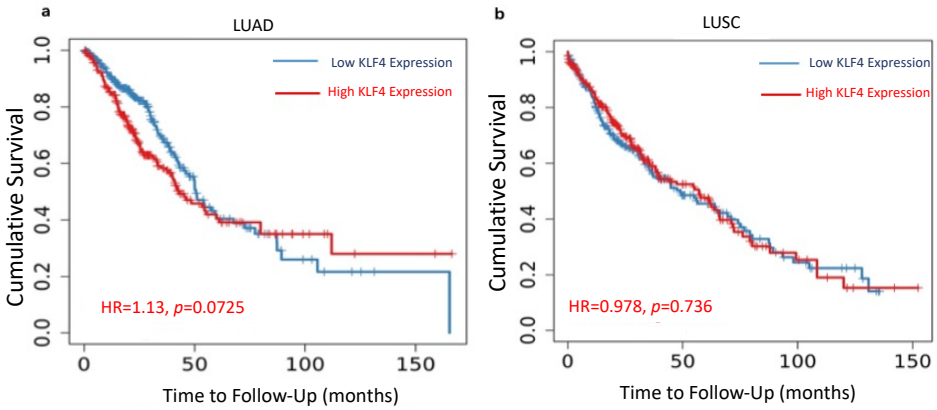

Figure 19. High KLF4 expression related to high survival (TIMER)

The survival curve showed the overall cause mortality of LUAD (a) and LUSC (b). They show that the high KLF4 expression related to high survival. Statistical analysis were determined using a two-tailed Student's *t*-test.

6. Discussion

In this study, we provided a novel gene therapy strategy for hypoxic/chronic lung disease caused by pulmonary hypertension (PH). In *in vitro* experiments, we used adeno-associated virus (AAV)-mediated overexpression of *Klf4* had an anti-inflammatory and anti-proliferative effect on endothelial cells (HUVECs) under hypoxic conditions. In *in vivo* experiments, it shows that overexpression of *Klf4* did not upregulate oncogenic genes (e.g., *p53*, *p21*, *p300*) in wide type mice. By using bioinformatic online databases, we found that the expression of *KLF4* is lower in lung cancer patients, compared to the health group. In summary, we provided a relevant theoretical support for the future use of *KLF4* as a gene therapy target.

6.1 AAV-mediated KLF4 overexpression *in vitro*

6.1.1 KLF4 overexpression promotes anti-inflammation

Previous studies have shown that human and mouse vascular endothelial cells express KLF4(23,30,53). KLF4 expression can be induced by shear stress and inflammatory cytokines, including TNF-α, IL-Iβ, and interferon-γ(34,54,55). Moreover, KLF4 inhibits inflammation by down-regulating MCP-1, VCAM, and TM and upregulating eNOS and TF in endothelial cells. The overall effect of KLF4 on inflammatory cells prompted us to explore the relationship between KLF4 and pulmonary hypertension, specifically hypoxia-induced/chronic lung disease-caused pulmonary hypertension (HPH/CHD-PH). In this study, we proved the anti-inflammatory potency of KLF4 overexpression under hypoxic conditions. As transcription factor, *KLF4* regulates downstream target genes' expression(31,56). Overexpressed KLF4 was bound to the *KLF4* DNA binding site in the promoters of *iNOS*, *TNF-α*, *MCP-1*, and *IL-6* genes and regulated the expression of these inflammatory mediators(31). We also showed that overexpression of KLF4 inhibited pro-inflammation. In other words, anti-inflammatory factors were activated by overexpression of *KLF4*.

6.1.2 KLF4 overexpression is associated with reduced (EndMT)

EndMT (Endothelia to Mesenchymal Transition) participates in the vascular remodeling associated with HPH/CDH-PH(8–10). SMCs (smooth muscle cells) causes abnormal vasoconstriction and increase, migrate and produce an extracellular matrix that contributes to structural remodeling, leading to pulmonary hypertension. The expression of α-SMA's (Alpha-smooth muscle actin) increases in response to hypoxic exposure. The features of

pulmonary hypertension are cellular changes in the walls of PAs. These changes consist of SM-like cells in previously non-muscularized vessels and thickening of the medial and anterior portions of muscular and elastic vessels(9). In the present study, we showed that the expressions of endothelial-associated factors (*CD31*, *vWF*, *Tie2*, *VE-cadherin*) were significantly decreased, and SMCs-associated markers (*α-SMA*, *SM22*, *vimentin*) was increased. KLF4 overexpression is associated with reduced EndMT in HUVECs.

The endothelium controls the exchange of solutes, hormones, and leukocytes between blood and tissues(10). Therefore, regulation of vascular endothelial permeability plays a critical role in many physiological and pathological processes, including development, tumor angiogenesis, and immunity and inflammation(8,9). Here, we showed that overexpression of KLF4 supports the vascular integrity and permeability. ZO-1 and VE-cadherin expressions were positively upregulated in KLF4 group under hypoxic conditions.

6.1.3 KLF4 overexpression preverves mitochondrial function

Mitochondrial dysfunction contributes to many diseases, including PH(11,12). In this study, overexpression of KLF4 shown a trend to improved mitochondrial metabolic function under hypoxia. However, the results were not statistical significance. It could be refined further in subsequent animal experiments to identify the correlation between KLF4 and mitochondrial function.

6.2 Establishment of KLF4 overexpression *in vivo*

6.2.1 *Klf4* overexpression in wide type mice

KLF4 is a known oncogenes(38,40). In this part, we clarified the safety of *Klf4* overexpression in wide type mice. Overexpression of *Klf4* five months after gene transduction, *p53*, *p21*, *p300* mRNA expression were not activated. Taken together, we could detect significant *EGFP* mRNA expression, but not AAV vector genomes, most probably due to lacking sensitivity to detecting low levels of AAV vector genomes 5 months after injection.

6.2.2 KLF4 expression in human samples by using Bioinformatic resouces

In gene therapy, safety is a particular concern. We performed a bioinformatics analysis based on multiple publicly available tumor database data. KLF4 expression was reduced in most tumor tissues, especially in the non-small cell lung cancer group, compared to normal lung tissue. By comparing the correlation between KLF4 expression levels and survival rate, we

found that the group with a high survival rate expressed higher levels of KLF4. Although these data did not reach statistical significance, they illustrated the feasibility of using KLF4 overexpression for gene therapy strategies.

7. Summary

Pulmonary hypertension (PH) is a severe cardiovascular disease with different pathogenetic causes. One of these causes is persistent low oxygen tension (hypoxia), resulting in pulmonary vascular inflammation and remodeling and, subsequently, blood flow impairment. As a result, the right ventricular blood pressure increases to overcome the decreased cross-section of pulmonary vasculature imposed by the pulmonary vascular constriction. Thus, understanding and modulating factors involved in pulmonary endothelial inflammation could contribute to potential therapeutic approaches. Krüppel-like factor 4 (KLF4) is a transcription factor expressed in the pulmonary vasculature endothelium, where it promotes anti-inflammatory and anticoagulant states and increases expression of endothelial nitric oxide synthase, a significant source of vasodilating nitric oxide. A novel role of endothelial KLF4 was discovered in the context of endothelial inflammation. Endothelial KLF4 has vasoprotective properties. Previous studies have also shown that an improved adeno-associated virus (AAV) vector enabled an efficient gene transfer into mice's pulmonary arterial endothelium, thereby allowing therapeutic modulation of gene expression.

In this study, we investigated the therapeutic potential of overexpression of the transcription factor KLF4 to prevent pulmonary hypertension. In vitro experiments were performed using AAV-mediated gene transfer of KLF4 into human umbilical vein endothelial cells (HUVECs) under hypoxic conditions. We analyzed inflammatory markers by real-time qPCR and Western blots. The results showed that overexpression of KLF4 had anti-inflammatory properties and contributed to the maintenance of endothelial barrier function. Besides this, overexpression of KLF4 inhibited the transition of endothelial cells to mesenchymal cells, improved mitochondrial function, and reduced the generation of reactive oxygen species (ROS). Subsequently, AAV vectors were used for KLF4 overexpression in pulmonary arteries in vivo. First, we aimed to demonstrate the efficiency and safety of overexpressing KLF4 in a mouse model. Overexpression of KLF4 did not cause apparent side effects in the murine model. Specifically, as KLF4 was shown to act as an oncogene regulator, overexpression of Klf4 did not activate oncogene (p53, p21, p300) expression. Overall, the AAV-mediated KLF4 overexpression enables significant protection of endothelial cells from hypoxia-induced stress in vitro and does not result in side effects when expressed in murine pulmonary artery endothelial cells in vivo. This study's results enable further investigations on AAV-mediated KLF4 overexpression in pulmonary artery endothelial cells in a murine model of chronic hypoxia-induced pulmonary hypertension.

8. Zusammenfassung

Die Pulmonale Hypertonie (PH) ist eine schwere Herz-Kreislauf-Erkrankung, zu deren Entwicklung unterschiedliche Ursachen führen können. Ein Grund ist eine niedrige Sauerstoffspannung (Hypoxie), die zu Entzündungen und Gefäßumbau und anschließend zu einer Beeinträchtigung des Blutflusses führt. Infolgedessen ist der Druck im rechten Ventrikel erhöht. Das Verständnis und die Modulation von Faktoren, die an einer endothelialen Entzündung beteiligt sind, könnten daher zur Entwicklung neuer therapeutischer Ansätze beitragen. Krüppel-ähnlicher Faktor 4 (KLF4) ist ein Transkriptionsfaktor, der im Gefäßendothel exprimiert wird, wo er entzündungs- und gerinnungshemmend wirkt und Zustände fördert. Kürzlich wurde eine neue Rolle von endothelialem KLF4 im Zusammenhang endothelialen Entzündungen entdeckt und gezeigt, dass endothelialer KLF4 ein vasoprotektive Eigenschaften hat. Daneben haben vorausgegangene Studien gezeigt, dass ein modifizierter Adeno-assoziierter Virus (AAV) -Vektor einen effizienten Gentransfer in Endothelzellen von Lungenarterien in Mäusen ermöglichte.

In dieser Studie sollte das therapeutische Potenzial einer Überexpression des Transkriptionsfaktors KLF4 zur Vorbeugung einer Pulmonalen Hypertonie untersucht werden. Zuerst wurde eine Überexpression von KLF4 durch AAV-vermittelten Gentransfers in Endothelzellen menschlicher Nabelschnurvenen (HUVECs) unter hypoxischen Bedingungen durchgeführt. Wir analysierten Entzündungsmarker mittels quantitativer PCR und Western Blots und konnten hierbei zeigen, dass eine Überexpression von KLF4 eine Reduktion von Entzündungsparametern bewirkte und die endotheliale Barrierefunktion aufrechterhielt. Darüber hinaus inhibierte die Überexpression von KLF4 auch den Übergang von Endothelzellen zu mesenchymalen Zellen und verbesserte die Mitochondrienfunktion. Die Erzeugung reaktiver Sauerstoffspezies in Endothelzellen wurde durch Überexpression von KLF4 reduziert. Anschließend sollte die Effizienz und Sicherheit eines KLF4 Gentransfers in einem Mausmodell untersucht werden. Hierzu wurden die bereits in vitro charakterisierten AAV-Vektoren zur -Überexpression in Lungenarterien in vivo verwendet. Wesentliche Nebenwirkungen durch die KLF4-Überexpression waren nicht ersichtlich. Obwohl KLF4 als Onkogenregulator wirken kann, führte die Überexpression nicht zur Aktivierung einer Onkogenexpression (p53, p21, p300). Zusammenfassend bilden die bisherigen Ergebnisse eine sichere Grundlage für weitere Untersuchungen zum therapeutischen Effekt einer AAV-vermittelten KLF4-Überexpression in einem präklinischen Lungenhochdruckmodell.

9. References

1. McDivitt JD, Barstow C. Cardiovascular Disease Update: Pulmonary Hypertension. FP Essent. 2017 Mar;454:24–8.
2. Mehari A, Valle O, Gillum RF. Trends in pulmonary hypertension mortality and morbidity. Pulm Med. 2014;2014:105864.
3. Frost A, Badesch D, Gibbs JSR, Gopalan D, Khanna D, Manes A, et al. Diagnosis of pulmonary hypertension. Eur Respir J. 2019 Jan 24;53(1):1801904.
4. Rosenkranz S, Preston IR. Right heart catheterisation: Best practice and pitfalls in pulmonary hypertension. European Respiratory Review. 2015 Dec;24(138):642-52.
5. Galiè N, Humbert M, Vachiery JL, Gibbs S, Lang I, Torbicki A, et al. 2015 ESC/ERS Guidelines for the diagnosis and treatment of pulmonary hypertension. Eur Heart J. 2016 Jan 1;37(1):67-119.
6. Hopkins N, McLoughlin P. The structural basis of pulmonary hypertension in chronic lung disease: remodelling, rarefaction or angiogenesis? J Anat .2002 Oct;201(4):335–48.
7. Ranchoux B, Harvey LD, Ayon RJ, Babicheva A, Bonnet S, Chan SY, et al. Endothelial dysfunction in pulmonary arterial hypertension: an evolving landscape. Pulm Circ. Jan-Mar 2018;8(1):2045893217752912.
8. Ranchoux B, Antigny F, Rucker-Martin C, Hautefort A, Péchoux C, Bogaard HJ, et al. Endothelial-to-mesenchymal transition in pulmonary hypertension. Circulation. 2015 Mar;131(11):1006–18.
9. Good RB, Gilbane AJ, Trinder SL, Denton CP, Coghlan G, Abraham DJ, et al. Endothelial to Mesenchymal Transition Contributes to Endothelial Dysfunction in Pulmonary Arterial Hypertension. Am J Pathol. 2015 Jul;185(7):1850-8.
10. Kovacic JC, Dimmeler S, Harvey RP, Finkel T, Aikawa E, Krenning G, et al. Endothelial to Mesenchymal Transition in Cardiovascular Disease: JACC State-of-the-Art Review. J Am Coll Cardiol. 2019 Jan;73(2):190-209.
11. Friedman JR, Nunnari J. Mitochondrial form and function. Nature. 2014 Jan 16;505(7483):335–43.
12. Fuhrmann DC, Brüne B. Mitochondrial composition and function under the control of hypoxia. Redox Biol.2017 Aug;12:208–15.
13. Eltzschig HK, Carmeliet P. Hypoxia and inflammation. N Engl J Med. 2011 Feb 17;364(7):656–65.
14. Lawrence T. The nuclear factor NF-kappaB pathway in inflammation. Cold Spring

Harb Perspect Biol. 2009 Dec;1(6):a001651.

15. Arthur Ataam J, Mercier O, Lamrani L, Amsallem M, Arthur Ataam J, Arthur Ataam S, et al. ICAM-1 promotes the abnormal endothelial cell phenotype in chronic thromboembolic pulmonary hypertension. J Heart Lung Transplant. 2019 Sep; 38(9): 982–996.
16. Galindo M, Santiago B, Alcami J, Rivero M, Martín-Serrano J, Pablos JL. Hypoxia induces expression of the chemokines monocyte chemoattractant protein-1 (MCP-1) and IL-8 in human dermal fibroblasts. Clin Exp Immunol. 2001 Jan;123(1):36–41.
17. Cook-Johnson RJ, Demasi M, Cleland LG, Gamble JR, Saint DA, James MJ. Endothelial cell COX-2 expression and activity in hypoxia. Biochim Biophys Acta. 2006 Dec;1761(12):1443–9.
18. Bonnet S, Boucherat O. The ROS controversy in hypoxic pulmonary hypertension revisited. Eur Respir J. 2018 Mar 8;51(3):1800276.
19. Jernigan NL, Naik JS, Weise-Cross L, Detweiler ND, Herbert LM, Yellowhair TR, et al. Contribution of reactive oxygen species to the pathogenesis of pulmonary arterial hypertension. PLoS One. 2017 Jun 30;12(6):e0180455.
20. Waypa GB, Smith KA, Schumacker PT. O2 sensing, mitochondria and ROS signaling: The fog is lifting. Mol Aspects Med. Feb-Mar 2016; 47–48:76–89.
21. van Gisbergen MW, Offermans K, Voets AM, Lieuwes NG, Biemans R, Hoffmann RF, et al. Mitochondrial Dysfunction Inhibits Hypoxia-Induced HIF-1α Stabilization and Expression of Its Downstream Targets. Front Oncol. 2020 May 19;10:770.
22. Ho JJD, Man HSJ, Marsden PA. Nitric oxide signaling in hypoxia. J Mol Med(Berl). 2012 Mar;90(3):217–31.
23. McConnell BB, Yang VW. Mammalian Krüppel-like factors in health and diseases. Physiol Rev. 2010 Oct;90(4):1337–81.
24. Chen ZY, Shie JL, Tseng CC. Gut-enriched Krüppel-like factor represses ornithine decarboxylase gene expression and functions as checkpoint regulator in colonic cancer cells. J Biol Chem. 2002 Nov 29;277(48):46831-9.
25. Brayer KJ, Kulshreshtha S, Segal DJ. The protein-binding potential of C2H2 zinc fingers domains. Cell Biochem Biophys. 2008;51(1):9-19.
26. Segre JA, Bauer C, Fuchs E. Klf4 is a transcription factor required for establishing the barrier function of the skin. Nat Genet. 1999 Aug;22(4):356-60.
27. Garrett-Sinha LA, Eberspaecher H, Seldin MF, de Crombrugghe B. A gene for a novel zinc-finger protein expressed in differentiated epithelial cells and transiently

in certain mesenchymal cells. J Biol Chem. 1996 Dec;271(49):31384–90.

28. Yet SF, McA'Nulty MM, Folta SC, Yen HW, Yoshizumi M, Hsieh CM, et al. Human EZF, a Kruppel-like zinc finger protein, is expressed in vascular endothelial cells and contains transcriptional activation and repression domains. J Biol Chem. 1998 Jan 9;273(2):1026-31.
29. Ghaleb AM, Laroui H, Merlin D, Yang VW. Genetic deletion of Klf4 in the mouse intestinal epithelium ameliorates dextran sodium sulfate-induced colitis by modulating the NF-κB pathway inflammatory response. Inflamm Bowel Dis. 2014 May;20(5):811–20.
30. Hamik A, Lin Z, Kumar A, Balcells M, Sinha S, Katz J, et al. Kruppel-like factor 4 regulates endothelial inflammation. J Biol Chem. 2007 May 4;282(18):13769-79.
31. Villarreal G, Zhang Y, Larman HB, Gracia-Sancho J, Koo A, García-Cardeña G. Defining the regulation of KLF4 expression and its downstream transcriptional targets in vascular endothelial cells. Biochem Biophys Res Commun. 2010 Jan 1;391(1):984-9.
32. Cowan CE, Kohler EE, Dugan TA, Mirza MK, Malik AB, Wary KK. Krüppel-like factor-4 transcriptionally regulates VE-cadherin expression and endothelial barrier function. Circ Res. 2010 Oct 15;107(8):959-66.
33. Yamaguchi S, Yamahara K, Homma K, Suzuki S, Fujii S, Morizane R, et al. The role of microRNA-145 in human embryonic stem cell differentiation into vascular cells. Atherosclerosis. 2011 Dec;219(2):468-74.
34. Fan Y, Lu H, Liang W, Hu W, Zhang J, Chen YE. Krüppel-like factors and vascular wall homeostasis. J Mol Cell Biol. 2017 Oct 1;9(5):352-363.
35. Shatat MA, Tian H, Zhang R, Tandon G, Hale A, Fritz JS, et al. Endothelial Krüppel-like factor 4 modulates pulmonary arterial hypertension. Am J Respir Cell Mol Biol. 2014 Mar;50(3):647-53.
36. Jaminon A, Reesink K, Kroon A, Schurgers L. The role of vascular smooth muscle cells in arterial remodeling: Focus on calcification-related processes. Int J Mol Sci. 2019 Nov 14;20(22):5694.
37. Shankman LS, Gomez D, Cherepanova OA, Salmon M, Alencar GF, Haskins RM, et al. KLF4-dependent phenotypic modulation of smooth muscle cells has a key role in atherosclerotic plaque pathogenesis. Nat Med. 2015 Jun;21(6):628-37.
38. Rowland BD, Peeper DS. KLF4, p21 and context-dependent opposing forces in cancer. Nature Reviews Cancer. 2006 Jan;6(1):11-23.

39. Ghaleb AM, Elkarim EA, Bialkowska AB, Yang VW. KLF4 suppresses tumor formation in genetic and pharmacological mouse models of colonic tumorigenesis. Mol Cancer Res. 2016 Apr;14(4):385-96.
40. Rowland BD, Bernards R, Peeper DS. The KLF4 tumour suppressor is a transcriptional repressor of p53 that acts as a context-dependent oncogene. Nat Cell Biol. 2005 Nov;7(11):1074-82.
41. Naso MF, Tomkowicz B, Perry WL, Strohl WR. Adeno-Associated Virus (AAV) as a Vector for Gene Therapy. BioDrugs. 2017 Aug;31(4):317-334.
42. Remes A, Basha DI, Puehler T, Borowski C, Hille S, Kummer L, et al. Alginate hydrogel polymers enable efficient delivery of a vascular-targeted AAV vector into aortic tissue. Mol Ther - Methods Clin Dev. 2021 Feb 24;21:83–93.
43. Atchison RW, Casto BC, Hammon WMD. Adenovirus-associated defective virus particles. Science (80-). 1965;
44. C. LB, A.M. D. Gene therapy progress and prospects - Vectorology: Design and production of expression cassettes in AAV vectors. Gene Ther. 2006;
45. Jungmann A, Leuchs B, Rommelaere J, Katus HA, Müller OJ. Protocol for Efficient Generation and Characterization of Adeno-Associated Viral Vectors. Hum Gene Ther Methods. 2017;28(5):235–46.
46. Bessis N, GarciaCozar FJ, Boissier MC. Immune responses to gene therapy vectors: Influence on vector function and effector mechanisms. Gene Therapy. 2004 Oct;11 Suppl 1:S10-7.
47. Varadi K, Michelfelder S, Korff T, Hecker M, Trepel M, Katus HA, et al. Novel random peptide libraries displayed on AAV serotype 9 for selection of endothelial cell-directed gene transfer vectors. Gene Ther. 2012 Aug;19(8):800-9.
48. Körbelin J, Sieber T, Michelfelder S, Lunding L, Spies E, Hunger A, et al. Pulmonary Targeting of Adeno-associated Viral Vectors by Next-generation Sequencing-guided Screening of Random Capsid Displayed Peptide Libraries. Mol Ther. 2016 Jun;24(6):1050–1061.
49. Pillay S, Zou W, Cheng F, Puschnik AS, Meyer NL, Ganaie SS, et al. Adeno-associated Virus (AAV) Serotypes Have Distinctive Interactions with Domains of the Cellular AAV Receptor. J Virol. 2017 Aug 24;91(18):e00391-17.
50. Brandes RP, Dueck A, Engelhardt S, Kaulich M, Kupatt C, De Angelis MT, et al. DGK and DZHK position paper on genome editing: basic science applications and future perspective. Basic Res Cardiol. 2021 Jan 15;116(1):2.

51. Müller OJ, Kaul F, Weitzman MD, Pasqualini R, Arap W, Kleinschmidt JA, et al. Random peptide libraries displayed on adeno-associated virus to select for targeted gene therapy vectors. Nat Biotechnol. 2003 Sep;21(9):1040-6.
52. Colella P, Ronzitti G, Mingozzi F. Emerging Issues in AAV-Mediated In Vivo Gene Therapy. Mol Ther Methods Clin Dev. 2017 Dec 1;8:87-104.
53. Shields JM, Christy RJ, Yang VW. Identification and characterization of a gene encoding a gut-enriched Krüppel-like factor expressed during growth arrest. J Biol Chem. 1996 Aug 16;271(33):20009–17.
54. Huertas A, Tu L, Humbert M, Guignabert C. Chronic inflammation within the vascular wall in pulmonary arterial hypertension: more than a spectator. Cardiovasc Res. 2020 Apr 1;116(5):885–93.
55. Lim CS, Kiriakidis S, Sandison A, Paleolog EM, Davies AH. Hypoxia-inducible factor pathway and diseases of the vascular wall. J Vasc Surg. 2013 Jul;58(1):219-30.
56. Schuetz A, Nana D, Rose C, Zocher G, Milanovic M, Koenigsmann J, et al. The structure of the Klf4 DNA-binding domain links to self-renewal and macrophage differentiation. Cell Mol Life Sci. 2011 Sep;68(18):3121-31.

10. Acknowledgement

I would like to thank everyone who has contributed to this work's success and supported me with words and deeds.

I would particularly like to thank my supervisor Prof. Dr. Oliver Müller, for enabling me to carry out the investigations as part of my dissertation in the working group's laboratory. Moreover, I would like to express my appreciation to Prof. Dr. Norbert Frey for providing an excellent environment in his department for molecular cardiology at Univesitätsklinikum Schleswig-Holstein, Campus Kiel. I would also like to thank Dr. Anca Remes for the always friendly patient instruction, and support with this project and the work appraisal.

I would like to appreciate the entire working group for molecular cardiology for the pleasant working atmosphere and the institute's wonderful time. I would particularly like to thank Susanne Hille, Christopher Borowski, Dima Ibrahim Basha, Marie Isabel Noormalal for the many exciting and stimulating discussions and the great time in and outside the laboratory. I also would like to thank Angela Schulz and Wiona Burmeister for the AAVs production that supported my study.
Besides, I also want to show my thanksgiving to my other friends in Germany, Tanya Sezin, Simge Yüz, Ling Ding etc. All their emotional support is the most valuable wealth during my study in a foreign country.

I am grateful to my family members and all my friends for their loving support over the years that made my doctoral study possible.

The doctoral degree is not the end but the beginning of something new. I believe that this memory will be the most precious one in my life.

11. Publications

- Xiaolu Ren, Yixun Zhang, **Yi Lyu**, et al. Lactate dehydrogenase and serum tumor markers for predicting metastatic status in geriatric patients with lung adenocarcinoma. Cancer Biomarker. 2019;26(2):139-150.
- J Hsu, FF Wang, **Yi Lyu**, et al. How mHealth apps improves access to cardiovascular care in Mainland China? European Heart Journal. 2018 Aug; Vol. 39(1): e565.
- Junjie Run, **Yi Lyu**, et al. Vasodilatory effect of midazolam on pre-contractions of in-vitro porcine coronary artery and its mechanisms. Chinese Pharmacological Bulletin 2017 Aug; 33 (8); 1131-5.
- **Yi Lyu**, Liu Jianzhou, et. Al. Case report: persistent fever with embolic events. Chin J Cardiovasc Med, April 2017, Vol. 22, No. 2.
- **Yi Lyu**, Jiyuan Lv. The relationship between body mass index and hypertension in teen-agers in Taiyuan. Modern Doctor of China 2010;130.